Universidad Zaragoza
1474

Trabajo Fin de Máster

Funcion de los microRNAS del tejido adiposo subcutaneo de las regulacion de la esteatosis hepatica.
Role of microRNAs in adipose tissue matabolism

Autor

José Andrés Castillo Rivas

Directores

Silvia Lorente Cebrián

José Miguel Arbonés Mainar

Master in Biophysics and Quantitative Biotechnology

FACULTAD DE CIENCIAS DE LA SALUD Y EL DEPORTE
2024–2025

Acknowledgments

Abstract

Table of contents

List of Tables

List of Figures

Chapter 1

Introduction and Antecedents

1.1 Overview of Hepatic Steatosis and Metabolic dysfunction-associated steatotic liver disease

Hepatic steatosis, defined by the excessive accumulation of triglycerides within hepatocytes, arises from a range of factors (Idilman et al., 2016). These include drug-induced effects, such as those caused by steroids and chemotherapy, infections like hepatitis C virus, and both nutritional and metabolic causes (Angulo, 2007). This condition is closely linked to steatotic liver disease (SLD), which encompasses two primary metabolic categories: alcoholic-related liver disease (ALD) and metabolic dysfunction-associated steatotic liver disease (MASLD) (Wong, 2024).

MASLD and its more advanced form, metabolic dysfunction-associated steatohepatitis (MASH), were previously known as nonalcoholic fatty liver disease (NAFLD) and nonalcoholic steatohepatitis (NASH), respectively (Mary et al., 2024). MASLD is diagnosed in adults who exhibit hepatic steatosis, identified through imaging techniques, blood biomarkers, or liver histology, in conjunction with being overweight or obese (Thyfault & Rector, 2020), or in the presence of type 2 diabetes mellitus (T2DM) or at least two metabolic risk abnormalities (hypertension, hyperlipidaemia or insulin resistance) (Chan et al., 2023; Z. M. Younossi, 2019). Although in many cases it may be asymptomatic in its early stages, this condition can progress to more severe stages depending on its cause (Ma et al., 2024). It encompasses a spectrum of liver pathologies ranging from simple hepatic steatosis to metabolic dysfunction-associated steatohepatitis (MASH), which is marked by lobular inflammation and hepatocellular ballooning, potentially progressing to fibrosis and cirrhosis, ultimately leading to liver failure (Sarwar et al., 2018).

The prevalence of MASLD is affecting more than a third of the adult population worldwide, making it the most common chronic liver disease globally (Miao et al., 2024). Among adults, the prevalence MASLD is approximately 30% (Z. M. Younossi et al., 2016). MASLD is particularly prevalent in overweight or obese individuals, with a global prevalence of approximately 50%, rising to nearly 60% in individuals with type 2 diabetes (T2D), a condition that affects up to 10% of the world's adult population (Z. M. Younossi et al., 2019).

Over the last 30 years, the global prevalence of MASLD has experienced significant growth, rising from 17.6% in 1990 to 23.4% in 2019, reflecting an average annual increase of approximately 1.0%. As of 2019, it was estimated that there were around 1.66 billion prevalent cases of MASLD worldwide (Paik et al., 2023). This condition is widespread, with the highest rates reported in South

America (44.4%), Middle East East and North Africa (36.5%) and followed by South Asia (33.8%), South-East Asia (33.1%), North America and Australia (31.2%), East Asia (29.7%), Asia Pacific regions (28.0%) and Western Europe (25.1%) (Z. M. Younossi et al., 2016, 2023). Approximately one-quarter of the European population is affected by this liver disease (Z. M. Younossi, 2019). In Europe, the prevalence of NAFLD variates between countries ranging from 5% to 44% (Z. Younossi et al., 2018). Data from Spain reflect similar rates, indicating a NAFLD prevalence of 25.8% in the adult population (Caballería et al., 2010).

This growing prevalence of MASLD is closely intertwined with the global rise in obesity and metabolic syndrome, conditions largely influenced by the complex interplay of adipose tissue function and dysfunction. Understanding the role of adipose tissue in metabolic regulation is therefore critical for elucidating the pathophysiology of MASLD.

1.2 Role of Adipose Tissue in Metabolic Regulation

1.2.1 Metabolic and Endocrine Functions of Adipose Tissue

Adipose tissue (AT) is a complex and dynamic organ with both metabolic and endocrine functions (Kershaw & Flier, 2004). It plays a pivotal role in energy balance, insulin sensitivity, immune responses and overall health (Rosen & Spiegelman, 2014). Its role extends beyond simple fat storage, influencing whole-body physiology and contributing to various pathologies, notably obesity and its associated complications like MASLD (Cinti, 2007).

1.2.2 Types and Location of Adipose Tissue

Adipose tissue in mammals exists in three primary forms: white adipose tissue (WAT), brown adipose tissue (BAT), and beige or brite (brown-in-white) adipose tissue. Each type is distinguished by its unique functions and cellular composition (Zwick et al., 2018). WAT primarily stores energy in the form of lipids, while BAT specializes in heat production through the uncoupling of oxidative phosphorylation, a process critical for thermogenesis (Cinti, 2019). Beige AT, a metabolically flexible tissue, can transition between energy storage and thermogenesis depending on physiological needs, highlighting its role in adaptive responses (Lopez-Yus et al., 2024).

Among these, WAT is the most abundant and metabolically versatile, playing a central role in maintaining energy homeostasis through lipid storage and mobilization (Lopez-Yus et al., 2024). Its key processes, lipogenesis (lipid synthesis) and lipolysis (lipid breakdown), are intricately regulated to meet the body's energy demands (Saponaro et al., 2015). WAT is the most abundant type of adipose tissue in the human body (Gesta & Kahn, 2017). The proportion of WAT can range from 5% to 60% of total body weight, with its distribution varying widely among individuals due to a combination of genetic and environmental factors (Lopez-Yus et al., 2024).

The anatomical distribution of WAT further underscores its functional diversity. WAT is primarily located in subcutaneous depots, beneath the skin, and visceral depots, surrounding internal organs such as the liver and intestines (Ghesmati et al., 2024). Additionally, smaller WAT depots are present in areas like bone marrow and muscle tissue, contributing to localized metabolic regulation (Cinti, 2019).

WAT is classified into two major subtypes based on location and function: - Subcutaneous white adipose tissue (scWAT): This type constitutes over 80% of total body fat and is predominantly

involved in long-term energy storage. Its distribution and metabolic activity play a protective role in overall metabolic health.

- Visceral white adipose tissue (visWAT): Accounting for 10–20% of total body fat in men and 5–10% in women, visWAT is more metabolically active and closely associated with adverse health outcomes such as insulin resistance and inflammation (Ibrahim, 2010; Jialal & Devaraj, 2018).

Understanding the distinct roles of scWAT and visWAT is essential for exploring their contributions to both physiological processes and the pathogenesis of metabolic diseases. This distinction sets the stage for examining how adipose tissue dysfunction, particularly in scWAT, influences conditions like MASLD.

1.3 Subcutaneous White Adipose Tissue (scWAT)

Subcutaneous White Adipose Tissue (scWAT) is the most abundant type of adipose tissue, found in various locations such as under the skin and in clustered regions of the body, including the upper (deep and shallow abdomen) and lower (gluteofemoral) body areas (Kwok et al., 2016).

Under physiological conditions, scWAT serves as a metabolically inert, long-term triglyceride storage site (McQuaid et al., 2010). Acting as a buffer for excess energy, scWAT protects other organs from ectopic lipid deposition and contributes to specific metabolic benefits (Zwick et al., 2018). This buffering role allows scWAT to mitigate the impact of excess dietary lipid consumption while also compensating for energy deficits during fasting, starvation, or strenuous exercise (McQuaid et al., 2010).

Structurally, scWAT is composed predominantly of adipocytes, which constitute approximately 50% of its cellular content (Koenen et al., 2021). In addition to adipocytes, scWAT includes vascular cells, fibroblasts, adipocyte precursors, multipotent mesenchymal stem-like cells, nerve processes, and immune cells such as macrophages, lymphocytes, eosinophils, and mast cells. These components are embedded within an extracellular matrix that provides structural support (Koenen et al., 2021). Collectively, these cells secrete a wide array of signaling molecules, including adipokines such as leptin, adiponectin, and resistin, which play essential roles in maintaining metabolic homeostasis (Lopez-Yus et al., 2024).

1.4 Metabolic Functions of WAT

The main role of white adipose tissue (WAT) is to manage energy balance by storing and releasing fatty acids (FAs) according to variations in energy availability (Lopez-Yus et al., 2024). Furthermore, WAT produces a range of hormones and cytokines, collectively referred to as adipokines, which are crucial for regulating numerous physiological functions (Scherer, 2006).

1.4.1 Lipids Storage and Mobilization

WAT maintains energy balance by storing and releasing fatty acids (FAs), a process controlled by the interplay between lipogenesis and lipolysis. This equilibrium is essential for sustaining energy homeostasis during periods of fasting or exercise (Lopez-Yus et al., 2024).

Lipogenesis is the process of synthesizing new lipids from excess glucose or dietary fatty acids. This process occurs in the cytoplasm of adipocytes and is tightly regulated by various hormones

and enzymes (Song et al., 2018). Insulin, the key hormone involved in this process, facilitates the uptake of glucose and fatty acids into adipocytes and activates essential enzymes for lipid synthesis, including acetyl CoA-carboxylase (ACC) and fatty acid synthase (FAS) (Carpentier, 2021).

Lipolysis, on the other hand, is responsible for breaking down stored lipids in adipose tissue to release energy for peripheral organs. This process is particularly important during fasting or exercise when glucose levels are low, prompting the body to utilize stored fat for energy (Grabner et al., 2021). Lipolysis is regulated by lipases, which are activated by signals from the sympathetic nervous system, primarily mediated by norepinephrine, with some influence from epinephrine. The primary lipases involved include adipose triglyceride lipase (ATGL), hormone-sensitive lipase (HSL), and monoacylglycerol lipase (MGL) (Duncan et al., 2007).

1.4.2 Endocrine Function

Additionally, WAT secretes various hormones and cytokines, collectively known as adipokines, which play essential roles in regulating multiple physiological processes such metabolic, inflammatory, and immune processes throughout the body (Scherer, 2006). The endocrine function of WAT is influenced by nutritional status, physical activity, hormonal levels, and environmental signals, and is closely related to its metabolic and storage functions (Scheja & Heeren, 2019).

Current understanding of adipose tissue (AT)-derived adipokines encompasses over 100 proteins that interact with various cells and tissues (Lopez-Yus et al., 2024). Leptin and adiponectin are the most prevalent and well-studied adipokines. Leptin, the first adipokine to be discovered, has been shown to influence appetite and energy expenditure, serving as an important feedback mechanism to the brain regarding the size and condition of adipose tissue (Friedman, 2019). In contrast, adiponectin promotes insulin sensitivity and fatty acid oxidation in skeletal muscle and the liver, contributing to the maintenance of glucose and lipid homeostasis (Karbowska & Kochan, 2006).

1.5 Dysregulation of Adipose Tissue and Its Implications

However, the function of scWAT is closely linked to body fat distribution, and under pathological conditions, its capacity to store lipids becomes overwhelmed. This dysfunction impairs its ability to store lipids appropriately, leading to hypoxia, infiltration of pro-inflammatory macrophages, and ectopic fat accumulation in other tissues like liver (Ipsen et al., 2018). These alterations directly contribute to the dysregulation of adipokine secretion, fostering a pro-inflammatory state and systemic insulin resistance, which are hallmark features in patients with NAFLD-associated diseases (Ipsen et al., 2018).

1.6 MicroRNAs y Regulación del Tejido Adiposo

1.6.1 microRNAS (miRNAs): biogenesis and function

MicroRNAs (miRNAs) have emerged as essential and versatile post-transcriptional regulators of gene expression, playing a significant role in various biological processes including the cell cycle, proliferation, lipid metabolism, inflammation, fibrosis among others (Santulli, 2015). The dysregulation of miRNA has been implicated in the pathogenesis of several many diseases and metabolic disorders, including NAFLD (Arrighetti & Beretta, 2021). Specific miRNAs are known to be differentially expressed in metabolic tissues, including adipose tissue, in response to pathological

states (Santulli, 2015). Their potential as biomarkers for disease progression and therapeutic targets has garnered significant interest in recent years (Arrighetti & Beretta, 2021).

Given the increasing prevalence of NAFLD and the limited availability of non-invasive diagnostic tools, identifying specific miRNAs as biomarkers in subcutaneous white adipose tissue could provide valuable insights into the underlying molecular mechanisms and aid in risk stratification. This study aims to bridge this knowledge gap by analyzing the differential expression of miRNAs in scWAT across varying degrees of steatosis, predicting their target genes, and exploring their potential functional roles. #### Basic nomenclature of the miRNA ### Relevancia en el metabolismo

Los miRNAs están implicados en procesos clave como la adipogénesis, la inflamación, la lipólisis y la resistencia a la insulina, todos fundamentales en la fisiopatología del tejido adiposo. ### MiRNAs en el contexto de MASLD: Evidencias crecientes sugieren que los miRNAs desempeñan un papel crucial en la comunicación entre el tejido adiposo y el hígado, influyendo en la progresión de la esteatosis hepática.

scWAT communicates with the liver and other metabolic organs through a network of signaling molecules, including adipokines, free fatty acids, and cytokines, which influence metabolic homeostasis (Ghesmati et al., 2024). Dysregulation of this crosstalk in the context of obesity and insulin resistance contributes to ectopic fat deposition and inflammation, exacerbating hepatic steatosis (Koenen et al., 2021).

1.6.2 Functional and Cellular Complexity of White Adipose Tissue

Beyond its anatomical distribution, the composition of WAT reveals a remarkable heterogeneity that underscores its functional complexity. While adipocytes are the primary cellular component, WAT also encompasses a rich network of blood vessels, nerve terminals, and various cell types, including immune cells. This cellular diversity plays a crucial role in supporting the tissue's metabolic and endocrine functions, further highlighting its central role in whole-body energy regulation (Kwok et al., 2016).

Chapter 2

Objectives

2.0.1 5. Study Hypothesis and Objectives

- Hypothesis based on the differential regulation of miRNAs according to steatosis grade and their impact on specific metabolic pathways.
- Main objectives, such as:
  - Identifying differentially expressed miRNAs in subcutaneous adipose tissue of patients with varying degrees of steatosis.
  - Predicting target genes of these miRNAs and analyzing their role in steatosis progression.
  - Assessing the feasibility of using these miRNAs as diagnostic or prognostic biomarkers.

Chapter 3

Methodological Framework

3.1 Input Data

The analyzed data corresponds to a FATe cohort of 78 obese patients with varying degrees of adiposity from subcutaneous adipose tissue (scWAT) samples. These samples are registered at the regional Biobank (Biobanco Aragón) and have previously obtained approval from CEICA. The patients in the FATe cohort are characterized by the following variables: sex, age, body mass index (BMI), steatosis, non-alcoholic steatohepatitis (NASH), hepatocytic ballooning, lobular inflammation, diabetes, hyperlipidemia, and non-alcoholic fatty liver disease (NAFLD).

3.1.1 Statistical Analysis

The results are expressed as median [interquartile range] and number (%). Pairwise group comparisons for continuous variables were calculated using Student's t-test for variables with a Gaussian distribution and the Mann–Whitney U test for data that do not follow this distribution. Categorical variables were analyzed using the chi-square test.

3.2 Analysis of sRNA-seq Data with *nf-core/smrnaseq*

For the analysis of small RNA sequencing (sRNA-seq) data, version 2.4.0 of the nf-core/smrnaseq pipeline (Peltzer et al., 2024) was used, which is specifically designed for the automated processing of microRNA data. This pipeline facilitates quality control, filtering, and quantification of microRNAs and their variants, and it was executed using the Docker profile to ensure reproducibility and compatibility across operating systems.

3.2.1 Execution of the *nf-core/smrnaseq* Pipeline

The installation of *nf-core/smrnaseq* was carried out following the instructions provided by the authors, available at https://nf-co.re/smrnaseq/2.4.0.

To ensure the proper installation and execution of the pipeline, the following key components were installed beforehand:

1. *Nextflow*: Version 24.04.4 of Nextflow was used, following the detailed instructions at https://nf-co.re/usage/installation.

2. *Java Runtime Environment (JRE)*: Version 11.0.25 of the Java Runtime Environment was installed, as it is required for compatibility with Nextflow and the *nf-core/smrnaseq* pipeline.

To ensure the reproducibility of results and facilitate pipeline execution, the authors recommend installing one of the available Docker containers. These containers include the necessary instructions and configurations for running the pipeline. This configuration is specified at runtime using the `profile` argument. In this analysis, the Docker image of *nf-core/smrnaseq*, available at https://hub.docker.com/r/nfcore/smrnaseq, was used.

The pipeline was executed on a server with 8 CPUs, 16 GB of RAM, and a Linux operating system. The following command was used in the terminal, which configures the main options, including the reference genome, input data, and output file location:

```
nextflow run nf-core/smrnaseq -r 2.4.0
-profile docker,ci
--genome GRCh38
--input '/home/joshoacr13/Documentos/TFM/nfcore-smrnaseq/input/samples.csv'
--fasta 'https://github.com/nf-core/test-datasets/raw/smrnaseq/reference/genome.fa'
--mirtrace_species 'hsa'
--outdir /home/joshoacr13/Documentos/TFM/nfcore-smrnaseq/workdir
-resume -c /home/joshoacr13/Documentos/TFM/nfcore-smrnaseq/nextflow_memory.config
--save_intermediates FALSE
```

The pipeline was executed three times due to the large number of samples, which exceeded the processing capacity of a system with these specifications.

3.2.2 Description of the Parameters Used

- `-profile docker,ci`: Runs the pipeline inside a Docker container to ensure reproducibility and sets up a continuous integration (CI) profile.
- `--genome GRCh38`: Specifies the human genome (version GRCh38) as the reference for sequence mapping.
- `--input`: Provides the path to the CSV file containing metadata and the paths to the FASTQ files.
- `--fasta`: URL to the FASTA file of the reference genome.
- `--mirtrace_species hsa`: Defines the species as Homo sapiens (hsa) for microRNA analysis with miRTrace.
- `--outdir`: Sets the working directory for the processed results.
- `-resume`: Allows continuation of a previous analysis without restarting from the beginning.
- `-c`: Specifies a custom configuration file (nextflow_memory.config) to adjust resource usage.
- `--save_intermediates FALSE`: Prevents the storage of intermediate files to save disk space.

3.2.3 Analysis Workflow and Tools Used

The *nf-core/smrnaseq* pipeline performs the following steps:

1. **Quality Control** An initial quality assessment of the raw reads was conducted using *FastQC* (version 0.12.1) (Andrews et al., 2010). Additionally, 3' adapter trimming was performed using *fastp* (version 0.23.4) (S. Chen et al., 2018), followed by quality and length filtering. A second quality assessment of the trimmed reads was conducted with *FastQC*.

2. **miRNA Quality Control** A more specific quality control for miRNAs was performed using *mirtrace* (version 1.0.1) (Kang et al., 2018). This tool allowed us to:

- **Verify Read Length Distribution**: The majority of reads fell within the expected range of 18–24 nucleotides, indicative of high-quality small RNA data.
- **Identify Contaminants**: Potential contaminants such as tRNA, rRNA, and other non-target molecules were flagged.
- **Taxonomic Classification**: Reads were classified taxonomically to ensure that most sequences originated from the organism of interest (*Homo sapiens*).

Samples that failed to meet the minimum quality thresholds, as determined by *mirtrace*, were excluded from further analysis to maintain data integrity and reliability.

3. **MicroRNA Quantification**:

- **Alignment**: The filtered reads were aligned against mature microRNA sequences in the miRBase database using *Bowtie1* (version 1.3.1)(Langmead et al., 2009). Unmapped reads were aligned against "hairpin" sequences to identify microRNA precursors.
- **Post-Alignment Processing**: *SAMtools* (version 1.16.1) (Danecek et al., 2021) was used to process the mapping results.
- **Quantification and Normalization**: Initial quantification was performed with *edgeR* (version 4.4) (Y. Chen et al., 2024), generating normalized count tables (TMM) for detected microRNAs. Exploratory graphs were generated, including a multidimensional scaling (MDS) analysis to cluster samples and a heatmap to evaluate similarities among them.

4. **IsomiR Annotation**: The collapsed reads were processed with *mirtop* (version 0.4.28) (Desvignes et al., 2020) to identify microRNA variants (isomiRs). This analysis allows for the mapping and annotation of variants related to length and sequence modifications of mature microRNAs.

The mirtop tool employs the Blending Analysis technique to process and integrate miRNA data, ultimately generating a count matrix that accurately represents the expression levels of these molecules in the analyzed samples. This method includes the following essential steps:

- **Read Grouping**: The miRNA reads are grouped from the processed data, ensuring that different variants and reference sequences are integrated coherently.
- **Adjustment for Variants**: Both miRNA variants (isomiRs) and standard reference sequences extracted from databases such as miRBase are considered. This adjustment is fundamental to obtaining an accurate representation of miRNA expression in the analyzed samples.

The application of *Blending Analysis* allows for the generation of a more robust and comprehensive count matrix, thus facilitating subsequent differential expression analysis.

5. **Analysis and Visualization of Results**: The overall pipeline metrics, encompassing quality assessments, mapping statistics, and expression analysis results, were consolidated and summarized using *MultiQC* (version 1.25.1) (Ewels et al., 2016). This versatile tool that aggregates output from various bioinformatics analyses into a unified, interactive report, enabling an efficient overview of the data processing workflow.

3.3 Differential expression analysis

3.3.1 Working Environment and Computational Resources

For the differential expression analysis, the R statistical software (R Core Team, 2024), version 4.4.1 (2024-06-14) (https://cran.r-project.org/), was used. This analysis was performed using the RStudio integrated development environment (IDE) (Posit team, 2023), version 2023.12.0+369, designed for Ubuntu Jammy (https://www.rstudio.com/).

The script used to perform the differential expression analysis is available in the file "`miRNA_steatosis.qmd`" which can be accessed at the following link: https://github.com/joshoandres13/miRNAs.

To execute this script, several libraries must be installed. Some of these are standard libraries available on CRAN, while others are specific to sequencing data analysis and are part of the Bioconductor project (Morgan, 2024) (https://www.bioconductor.org/, version 3.19.1).The libraries utilized in this analysis include *isomiRs*(Pantano & Escaramis, 2024) and *DESeq2* (Love et al., 2014), both of which are part of Bioconductor.

3.3.2 Data Import and Preparation

The starting data consisted of `.tsv` format files generated by the *mirtop* tool, which is integrated into the *nf-core/smrnaseq* pipeline. These files contained raw isomiR counts for each sample. They were then imported into R and combined into a single count matrix, where:

- Rows represent the identified isomiRs.
- Columns correspond to the experimental samples.

Additionally, a metadata matrix was created to describe the experimental conditions of each sample, including variables such as `sex` and `steatosis`.

Using the *mirtop* count matrix and the metadata matrix, an object of class `IsomirDataSeq` was created. This object is fundamental within the *isomiRs* package, as it allows for efficient management of the information derived from small RNA sequencing studies, facilitating differential expression analysis and the interpretation of biological results.

3.3.3 Filtering and Processing of isomiRs

3.3.3.1 Filtering of isomiRs with Low Read Counts

The filtering process allows for the grouping of isomiRs into different categories, assigning them to a single variant associated with a miRNA. This grouping is crucial to ensure consistency and accuracy in differential expression analyses.

To minimize technical noise in the data and focus on biologically relevant signals, a strict filtering criterion was applied. Only isomiRs with at least 20 reads in at least 40 samples were retained. This step is essential to eliminate sequences with low representation that could affect the robustness of subsequent analyses.

3.3.4 Gene Expression Data Analysis

Gene expression analysis was conducted using the *DESeq2* package in R, which models count data and performs statistically robust tests to identify significant differences in gene expression. The

analysis steps are outlined below:

3.3.4.1 Data Preparation

The analysis began with the creation of a `DESeqDataSet` object from a count matrix and a metadata table describing the experimental conditions. In this case, the count matrix contained expression data for isomiRs (variants of a single RNA), and the experimental design included two variables: **sex** and **steatosis**.

3.3.4.2 Model Fitting

To evaluate the effect of steatosis on isomiR expression, a full model including both variables was fitted. A reduced model excluding the steatosis variable was then fitted, allowing a comparison between the two models using the Likelihood Ratio Test (LRT).

3.3.4.3 Obtaining Results

The results of the analysis were obtained using the `results()` function, which provides a data frame containing information about log2 fold changes and adjusted p-values.

3.3.4.4 Filtering Significant Results and Visualization

The criteria established to identify significant isomiRs:

- *Strict criterion*: Selected isomiRs with an adjusted p-value (padj) less than 0.05 and an absolute log2 fold change greater than 1 for the higly expresed and less than 1 for the less expressed.

To facilitate result interpretation, a scatter plot was generated showing log2FoldChange on the x-axis and -log10 p-value on the y-axis. Points were colored red to indicate significant isomiRs and black for non-significant ones. The significants will be used in the following steps.

3.4 Target mRNA Selection and Validation Using *multiMiR*

The identification of mRNA targets was performed using the *multiMiR* bioinformatics package (Ru et al., n.d., 2014), version 2.4.0 in R. *multiMiR* facilitates systematic search and annotation of microRNA targets, providing functional analysis to elucidate biological mechanisms. For this analysis, only validated interaction data were used.

3.4.1 Filtering Parameters

The validated target table provided by *multiMiR* was used during the selection process. Key columns included:

1. **database**: Source database of validated interactions, such as *miRTarBase*, *TarBase*, or *miRecords*.
2. **mature_mirna_id**: Standard format identifier for the miRNA.
3. **target_symbol**: Target gene symbol.
4. **experiment**: Experimental methods used for validation, including luciferase assays, Western blot, or qRT-PCR.

5. **support_type**: Level of experimental support, such as "Functional MTI" (miRNA-mRNA functional interaction).
6. **pubmed_id**: References to PubMed articles reporting the interaction.
7. **type**: Specifies whether the interaction is "validated" or "predicted."

3.4.2 Selection Criteria

To ensure reliable results, databases were filtered according to update criteria and the following selection parameters:

- Databases up-to-date at the time of analysis were prioritized (*miRTarBase* and *TarBase*).
- Only interactions classified as "validated" were included.
- Interactions backed by robust experimental methods, such as luciferase assays or Western blot, were prioritized.
- Interactions with functional support ("Functional MTI") and verifiable references in PubMed were selected.

This approach ensured the identification of mRNA targets with high reliability and experimental backing, facilitating the analysis of potential regulatory functions of the studied miRNAs.

3.4.3 Functional Analysis

To explore biological functions associated with validated target genes, Gene Ontology (GO) enrichment analysis was conducted using the *clusterProfiler* package (Xu et al., 2024) in R. This analysis identified biological processes, molecular functions, and cellular components involving miRNA-regulated genes.

1. **Data Preparation**:
   - Symbols for validated genes (*target_symbol*) associated with selected miRNAs were extracted using *multiMiR*, with duplicates removed.
2. **GO Enrichment Analysis**:
   - The `enrichGO()` function from *clusterProfiler* was used with the following parameters:
     - `OrgDb`: Human gene database from *org.Hs.eg.db* (Carlson, 2024).
     - `keyType`: Key type defined as "SYMBOL".
     - `ont`: Ontology type analyzed, including "ALL" (biological processes, molecular functions, and cellular components).
     - `pAdjustMethod`: False discovery rate (FDR) adjustment method using Benjamini-Hochberg.
     - `qvalueCutoff` and `pvalueCutoff`: Cutoff values set to 0.05 to select significant results.
3. **Results and Visualization**:
   - A bar plot of the top 10 enriched categories in biological processes (GO:BP) was generated, showing statistical significance and the number of genes associated with each category.
   - The plot highlighted key biological processes related to the activity of miRNA target genes.

Chapter 4

Results

4.1 Stastical Analysis

In the following Table 4.1 is described the FATe cohort that consist of 78 obese patients aged between 22 and 61 years (mean age: 47.03 ± 9.33 years) with an average body mass index (BMI) of 46.11 ± 6.13 kg/m², was evaluated for multiple clinical characteristics, including the degree of hepatic steatosis, lobular inflammation, and the prevalence of associated metabolic diseases. According to the hepatic fat scale, 35.9% of patients had less than 5% liver fat, indicating a normal or minimal steatosis state. A total of 32.1% exhibited mild steatosis (5–33%), while 25.6% showed moderate fat accumulation (33–66%). Only 6.4% of patients presented severe steatosis (>66%), with no significant differences between men and women (p=0.818).

Table 4.1: Clinical characteristics of the FATe cohort and their statistical differences. Data are presented as number (%) or median [interquartile range]. Differences between groups were tested with the Mann–Whitney U test and chi-square test; *BMI*: Body Mass Index (kg/m²); *NASH*: Non-alcoholic steatohepatitis.

Characteristic	**Overall (n=78)**	**Female (n=59)**	**Male (n=19)**	**p test**
Age (years) median [IQR]	47.03 (13.75)	46.53 (13)	48.58 (14)	0.408
Body Mass Index (kg/m²) median [IQR]	46.11 (8.70)	45.68 (8.76)	47.42 (8.70)	0.284
NAFLD Activity Score Category (%):				0.510
- 0	22 (28.2)	16 (27.1)	6 (31.6)	
- 1	16 (20.5)	13 (22.0)	3 (15.8)	
- 2	17 (21.8)	14 (23.7)	3 (15.8)	
- 3	9 (11.5)	7 (11.9)	2 (10.5)	
- 4	9 (11.5)	7 (11.9)	2 (10.5)	
- >= 5	5 (6.4)	2 (3.4)	3 (15.8)	
Hepatic Steatosis Scale (%):				0.818
- < 5%	28 (35.9)	21 (35.6)	7 (36.8)	
- 5-33%	25 (32.1)	20 (33.9)	5 (26.3)	
- > 33-66%	20 (25.6)	15 (25.4)	5 (26.3)	
- > 66%	5 (6.4)	3 (5.1)	2 (10.5)	
Hepatocytic ballooning Category (%):				0.489
- None	58 (74.4)	45 (76.3)	13 (68.4)	

- Few cells	13 (16.7)	10 (16.9)	3 (15.8)	
- Many cells	7 (9.0)	4 (6.8)	3 (15.8)	
Lobular Inflammation Category (%):				0.596
- No foci	52 (66.7)	41 (69.5)	11 (57.9)	
- < 2 foci/200x	19 (24.4)	14 (23.7)	5 (26.3)	
- 2-4 foci/200x	4 (5.1)	2 (3.4)	2 (10.5)	
- > 4 foci/200x	3 (3.8)	2 (3.4)	1 (5.3)	
Diabetes:				1.000
- Yes (%)	21 (26.9)	16 (27.1)	5 (26.3)	
- No (%)	57 (73.1)	43 (72.9)	14 (73.7)	
Hyperlipidemia:				0.006
- Yes (%)	27 (34.6)	15 (25.4)	12 (63.2)	
- No (%)	51 (65.4)	44 (74.6)	7 (36.8)	
Non-alcoholic steatohepatitis:				0.249
- NASH (%)	12 (15.4)	7 (11.9)	5 (26.3)	
- Non-NASH (%)	66 (84.6)	52 (88.1)	14 (73.7)	

Regarding lobular inflammation, most patients (66.7%) had no inflammatory foci, while 24.4% exhibited fewer than two foci per microscopic field, and 3.8% showed severe inflammation (>4 foci). Hepatocyte ballooning analysis revealed that 74.4% of patients did not display significant damage, although 9.0% showed severe ballooning.

Among metabolic comorbidities, 26.9% of patients were diagnosed with diabetes, and 34.6% presented hyperlipidemia, with the latter being significantly more prevalent in men (63.2%) compared to women (25.4%, p=0.006). Additionally, 15.4% of patients were classified with non-alcoholic steatohepatitis (NASH), although this proportion showed no statistically significant differences between genders (p=0.249). Collectively, these data highlight the heterogeneity in the clinical characteristics of the cohort, emphasizing the complexity of the relationship between obesity and liver disease in this group of patients.

4.2 Quality Control Analysis

The quality control analysis using the *FastQC* tool, integrated into the nf-core/smrnaseq pipeline, allows for the evaluation of the samples both before and after processing with *fastp*, a rapid tool for preprocessing DNA sequencing data that includes adapter trimming, quality filtering, and report generation. This procedure is essential for verifying whether the sample quality is adequate. In general terms, the Table 4.2 shows a descriptive analysis with metrics related to sequencing data.

Table 4.2: Descriptive statistics of the analyzed metrics with fastp. *% Duplication*: Duplication rate before filtering; *Reads After Filtering*: Total reads after filtering in millions; *% GC* content: GC content after filtering; *% PF*: Percent reads passing filter; *% Adapter*: Percentage adapter-trimmed reads

	Mean	**sd**	**Median**	**Minimum**	**Maximum**	**Range**
% Duplication	98.30513	0.68	98.45	94.31	99.09	4.78
Reads After Filtering (M)	25.23152	5.67	25.82	1.51	35.47	33.96
% GC content	46.71982	1.68	46.43	43.26	50.89	7.63

% PF	99.02358	1.21	99.36	90.13	99.76	9.63
% Adapter	99.38240	0.35	99.45	96.96	99.62	2.66

The metrics obtained from the fastp analysis provide a detailed overview of the preprocessing performance across the samples. The percentage of duplicated reads before filtering was notably high, with a mean of 98.31% (±0.68), a median of 98.45%, and a range between 94.31% and 99.09%. After filtering, the number of reads retained per sample averaged 25.23 million (±5.67M) suggesting a reasonable amount of reads obtained, with a median of 25.82M and a range from 1.51M to 35.47M.

The GC content showed consistency across the samples, with an average of 46.72% (±1.68), a median of 46.43%, and a range between 43.26% and 50.89%. The percentage of pass-filtered (PF%) reads was high, with an average of 99.02% (±1.21), reaching a maximum of 99.76%, as shown in Figure 4.1 .Similarly, adapter trimming was highly effective, achieving a mean success rate of 99.38% (±0.35) indicating a low level of adapter contamination in most samples, and a range from 96.96% to 99.62%. These results confirm the efficiency of the preprocessing steps, ensuring that high-quality reads were retained while effectively removing low-quality sequences and adapters.

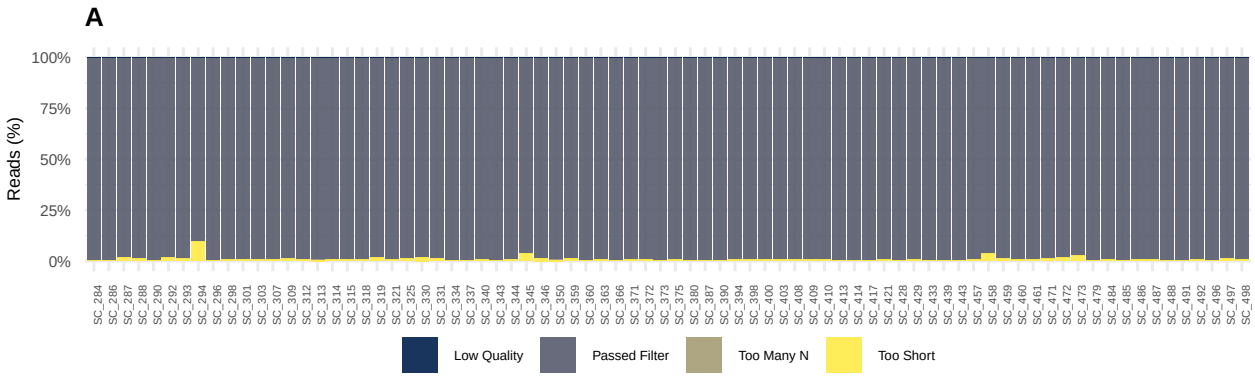

Figure 4.1: Fastp: Filtered Reads

In the analysis of the mean quality value of sequences across all bases using *fastp*, both before and after trimming, it is evident from Figure 4.2 (*A* and *B*)that the sequences from all samples consistently fall within an acceptable quality range, with mean Phred scores exceeding 30. This indicates a high base-calling accuracy, with an error probability of less than 0.1%, ensuring robust data integrity throughout the process.

Regarding the metric of the average quality value of each sequence (Phred score) across all samples Figure 4.2 (*C* and *D*), the values consistently exceed 30, with most samples achieving scores around 35. These results indicate that the average sequence quality is optimal, ensuring high reliability and low error rates in all cases.

In the analysis of the GC content per sequence, it is observed that, prior to trimming, none of the samples exhibit an ideal GC profile Figure 4.2 (*E* and *F*). However, post-trimming, the GC content improves as the percentage decreases, aligning more closely with expected values. Additionally, no issues with the presence of ambiguous bases (Ns) are detected in any of the samples Figure 4.2 (*G* and *H*).

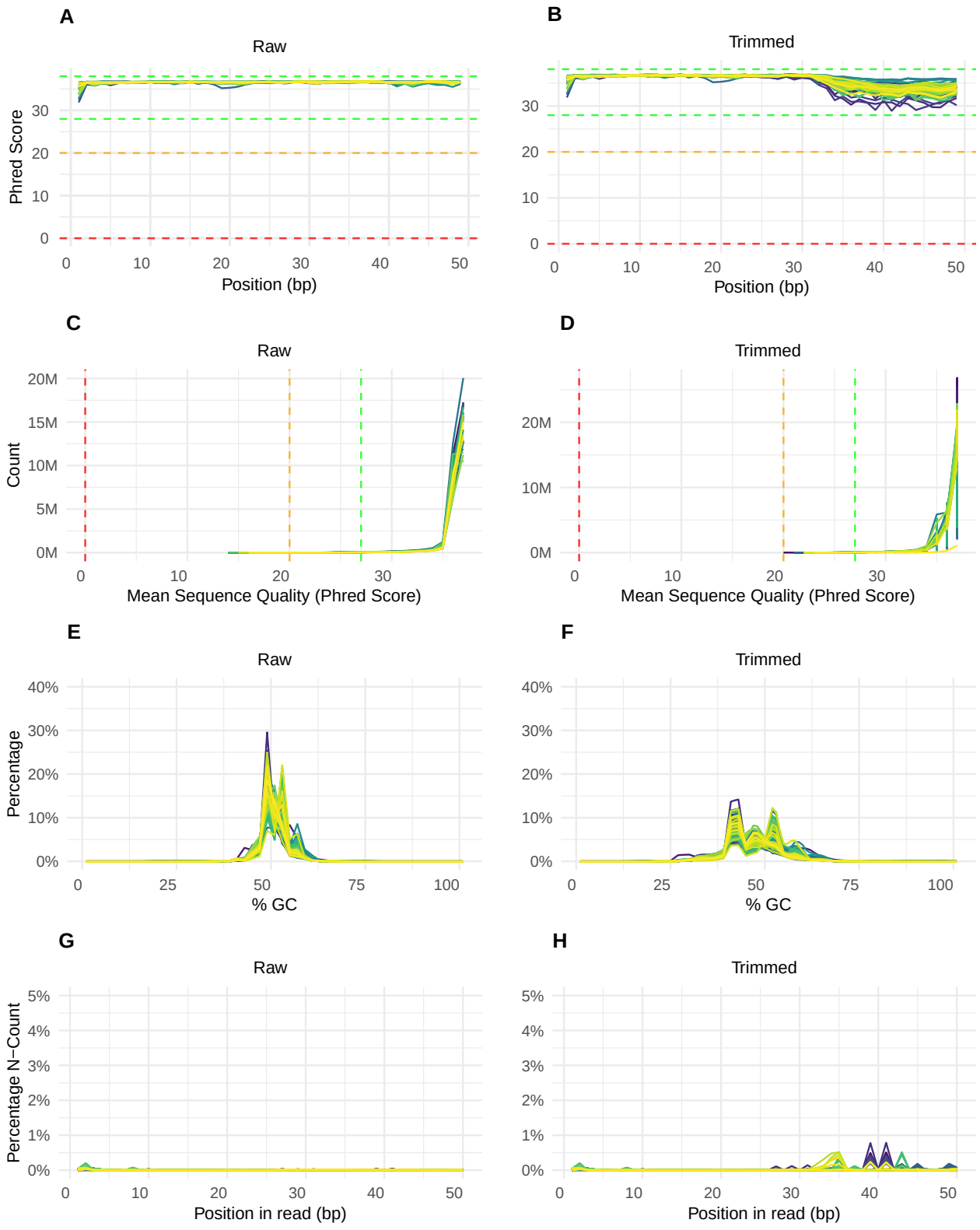

Figure 4.2: FastQC (v0.12.1) Analysis. *A* and *B*: Mean quality values of sequences across all bases after and before using fastp (v0.23.4); *C* and *D*: Per Sequence Quality Scores across all bases after and before using fastp; *E* and *F*: Per Sequence GC Content Raw after and before using fastp; *G* and *H*: Read N content after and before using fastp.

However, the distribution of sequence lengths is irregular across all samples Figure 4.3. The majority of sequences cluster around a length of 20-25 nucleotides, although a smaller subset of sequences with lengths between 29-32 nucleotides is also observed.}

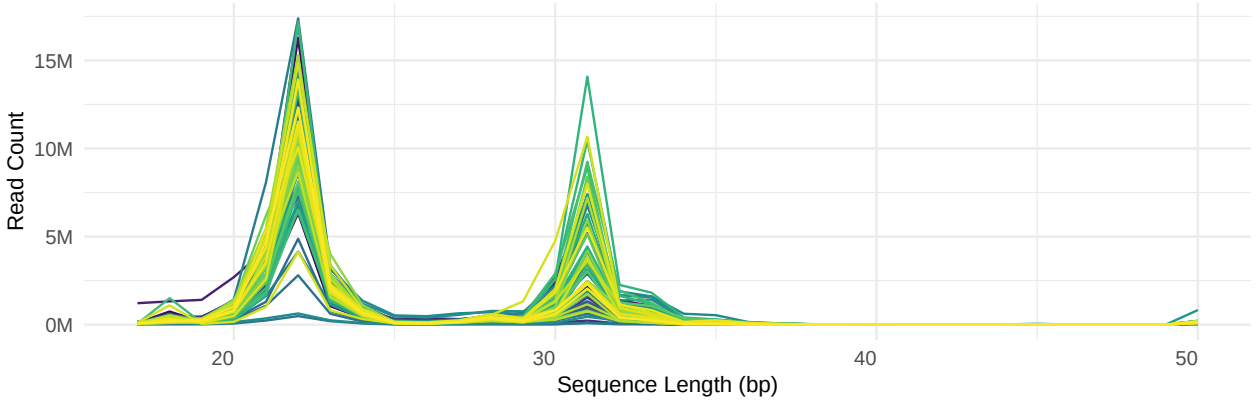

Figure 4.3: FastQC: Sequence Length Distribution

In the Figure 4.4 shows the total number of reads per sample is around 25 million, both in Raw and Trimmed, with means of 25.47 and 25.23 million, respectively. The interquartile ranges (IQR) of these measurements are similar, approximately 4.2 million, reflecting a high consistency among the samples.

Regarding duplicate reads, they dominate the data, with means of 25.10 million in Raw and 24.95 million in Trimmed, and an IQR of about 4.2 million in both conditions. This indicates that more than 90% of the sequences are duplicated, a high value but expected in smRNAseq samples, given the nature of the short reads of 20 to 30 nucleotides.

In contrast, unique reads are significantly less frequent, with means of 0.38 million in Raw and 0.28 million in Trimmed. The interquartile ranges for these measurements are also low, around 0.13 million in Raw and 0.10 million in Trim.

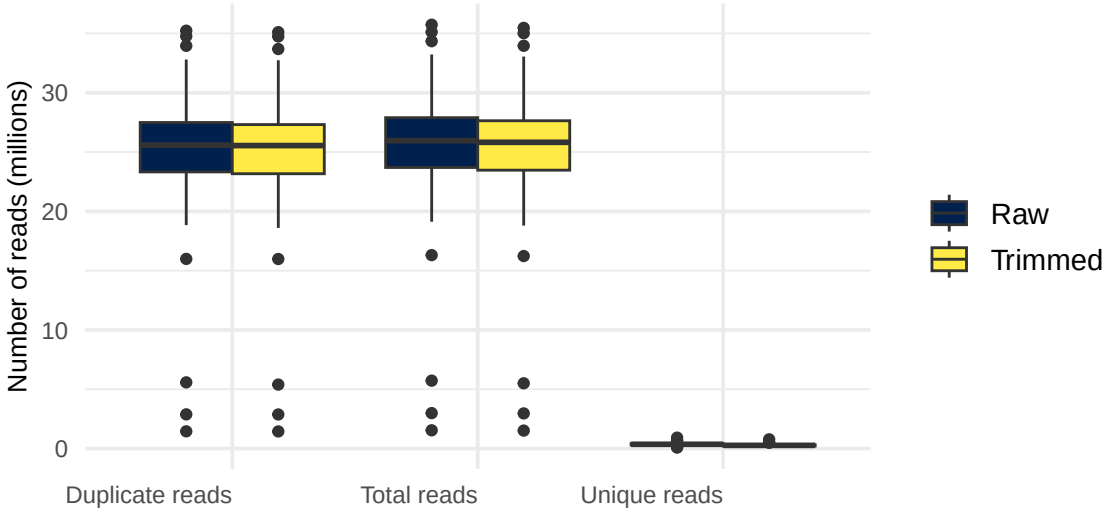

Figure 4.4: Number of reads from small RNA-seq. Total reads before and after trimming of adapters

An important aspect observed in the quality results is the successful removal of adapters. Running *FastQC* on the original files enabled the identification of the adapters used in library construction, specifically the Illumina Universal Adapter type, which is designed to facilitate the amplification and sequencing of a wide range of sample types. Using fastp, these adapters have been effectively removed from all samples, as shown in Figure 4.5

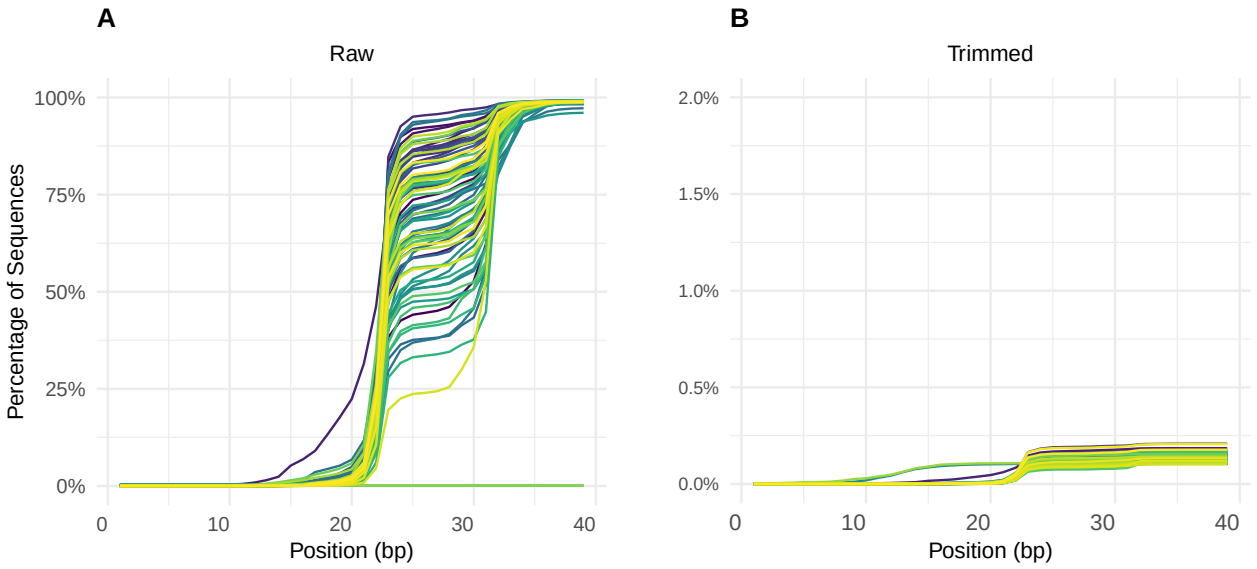

Figure 4.5: Detection (A) and removal (B) of the adapter using fastp (version 0.23.4)

4.3 MicroRNA Quantification

In this step of the *nf-core/smrnaseq pipeline*, the alignment of the reads is performed, initially against databases of mature and precursor miRNAs sequentially. These alignments enable the identification and quantification of miRNAs. The statistics obtained for mature miRNAs, precursor miRNAs, and the combination of both against the reference genome are presented in Table 4.3. On average, 52.07% of the mature miRNAs were mapped, with a range between 17.72% and 79.74%.

For precursor miRNAs, an average of 32.33% of sequences was identified, ranging from 6.31% to 68.83%. Subsequently, the reads of mature and precursor miRNAs were aligned against a reference genome, not for miRNA identification and quantification but as a quality control for the sequences. In this regard, the mean percentage of aligned reads was around 43% of the total reads. Across the sample set, minimum values of 10.27% and maximum values of 73.31% were observed. For more details, the metrics for each sample can be found in (Appendix A,B and C).

Table 4.3: Descriptive statistics of alignment with samtools of all samples. TM: Mean of Total Mapped (reads); TU: Mean od Total Unmapped (reads): Mean M: Mean Mapped (%); Max M: Max Mapped (%); Min M: Min Mapped (%)

Group	TM	TU	Mean M	Max M	Min M
mature	13166950	12194855	52.07395	79.74903	17.722429
mature_hairpin	3644435	8836242	32.33440	68.83115	6.311741
mature_hairpin_genome	4334118	4565712	43.86662	73.31495	10.279240

4.4 IsomiR Annotation

Mirtop (v0.4.28) was used for the annotation of miRNAs and isomiRs and to calculate general statistics. In Figure 4.6 (A), the read counts of isomiRs are shown, consisting of the total aligned read counts for each type of isomiR detected across all miRNAs. Of the total annotated miRNA sequences per sample, an average of approximately 59% corresponds to *Reference miRNA*, with values ranging from 36.70% to 71.66%.

This is followed by sequences belonging to the *3' Isoform*, with an average of 21.28% and a range of 14.26% to 32.22%. Similarly, sequences corresponding to the *3' Addition* isoform present an average of 14.81%, ranging from 10.00% to 27.03%. Sequences of the *5' Isoform* were detected with an average of 4.05%, ranging from 2.84% to 8.42%. Finally, other isoforms were found at percentages below 0.5%.

In Figure 4.6 (B), the unique read counts for isomiRs are displayed, representing the number of distinct sequences identified for each isomiR type across all miRNAs. Among the total unique miRNA sequences per sample, an average of 32.25% corresponds to the *3' Isoform*, with values ranging from 31.05% to 34.68%. This is followed by 24.46% of *3' Addition* sequences, 13.19% of *5' Isoform* sequences, and 10.74% of sequences with single nucleotide variations (SNVs) in the Seed Region (*SNV in Seed Region*).

Additionally, 8.71% of the unique sequences correspond to *Supported SNVs in the Central Region*, 7.45% to *SNVs in the Central Region*, and 1.93% to *SNVs in the Central Offset Region*. Finally, only 1.22% of the unique sequences align with *Reference miRNAs*. Among these unique sequences of *Reference miRNAs*, the samples exhibit an average of approximately 618 sequences, with values ranging from 323 to 801 sequences.

In figure Figure 4.6 (C), the *mean isomiR read counts* are presented, which refer to an average calculation that helps describe how the reads of isomiRs are distributed within a dataset. Among the annotated isomiR sequences per sample, the *reference miRNA* accounts for 96.51%, with ranges varying from 88.70% to 98.13%. On the other hand, the distributions of isomiR variants are as follows: *3' Isoform* (1.36%), *3' Addition* (1.23%), *5' Isoform* (0.64%), *SNVs in the Central Offset Region* (0.05%), *SNVs in the Central Region* (0.06%), *Supported SNVs in the Central Region* (0.05%), and *SNV in Seed Region* (0.05%), all of which are below 1.40%.

4.5 miRNA Quality Control

The *nf-core/smrnaseq* pipeline performs a quality analysis specific to smRNAseq data using miRTrace. miRTrace conducts adapter trimming and discards low-quality reads in the quality control (QC) filters. This analysis assesses sequencing quality, identifies the presence of miRNA and unwanted sequences from tRNA, rRNA, or Illumina artifact sequences, and identifies clade-specific miRNA profiles based on a comprehensive catalog of previously identified miRNA families.

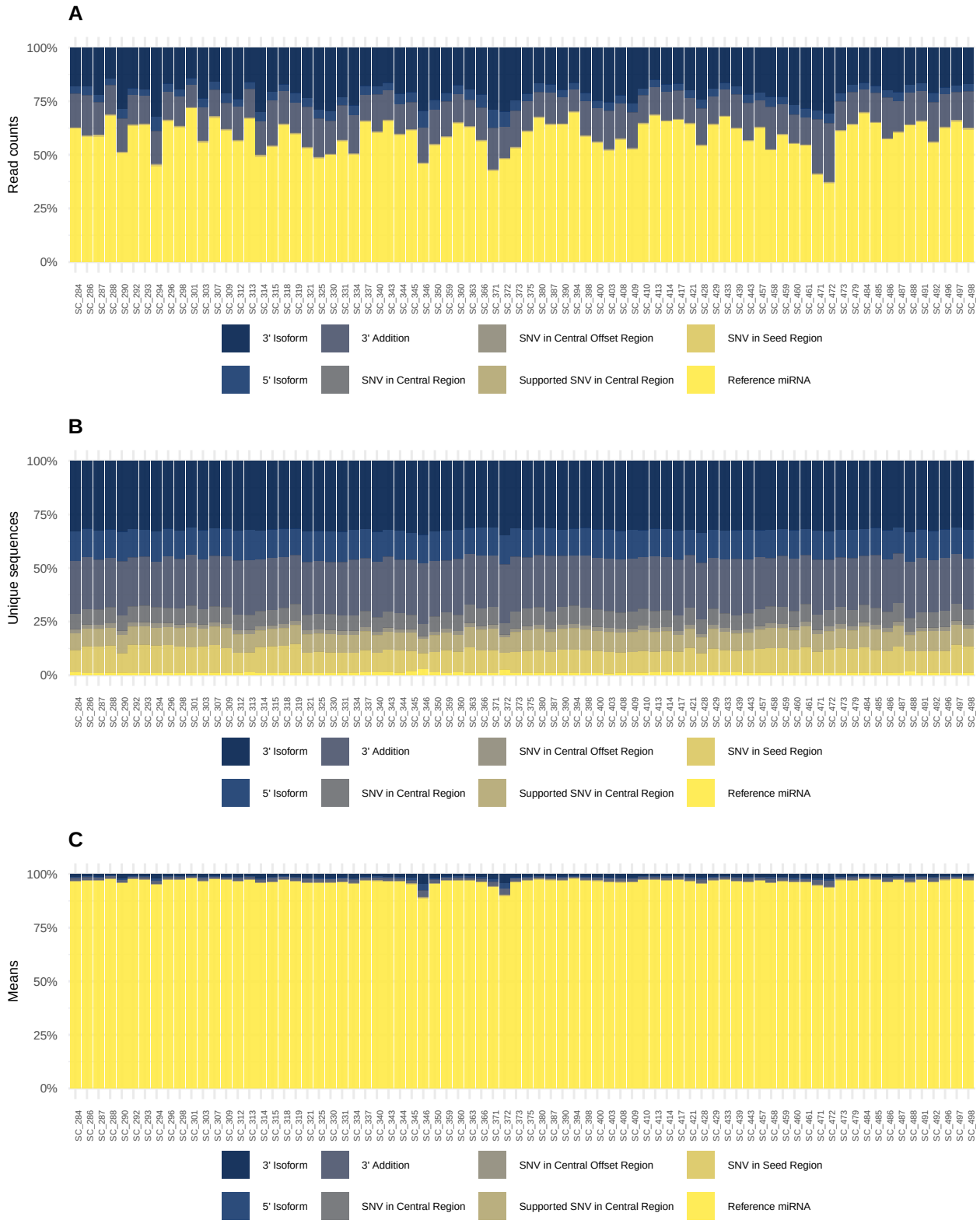

Figure 4.6: Annotation of miRNAs and isomiRs with mirtop (v0.4.28). *A*: IsomiR read counts; *B*: IsomiR unique read counts; *C*: Mean isomiR read counts

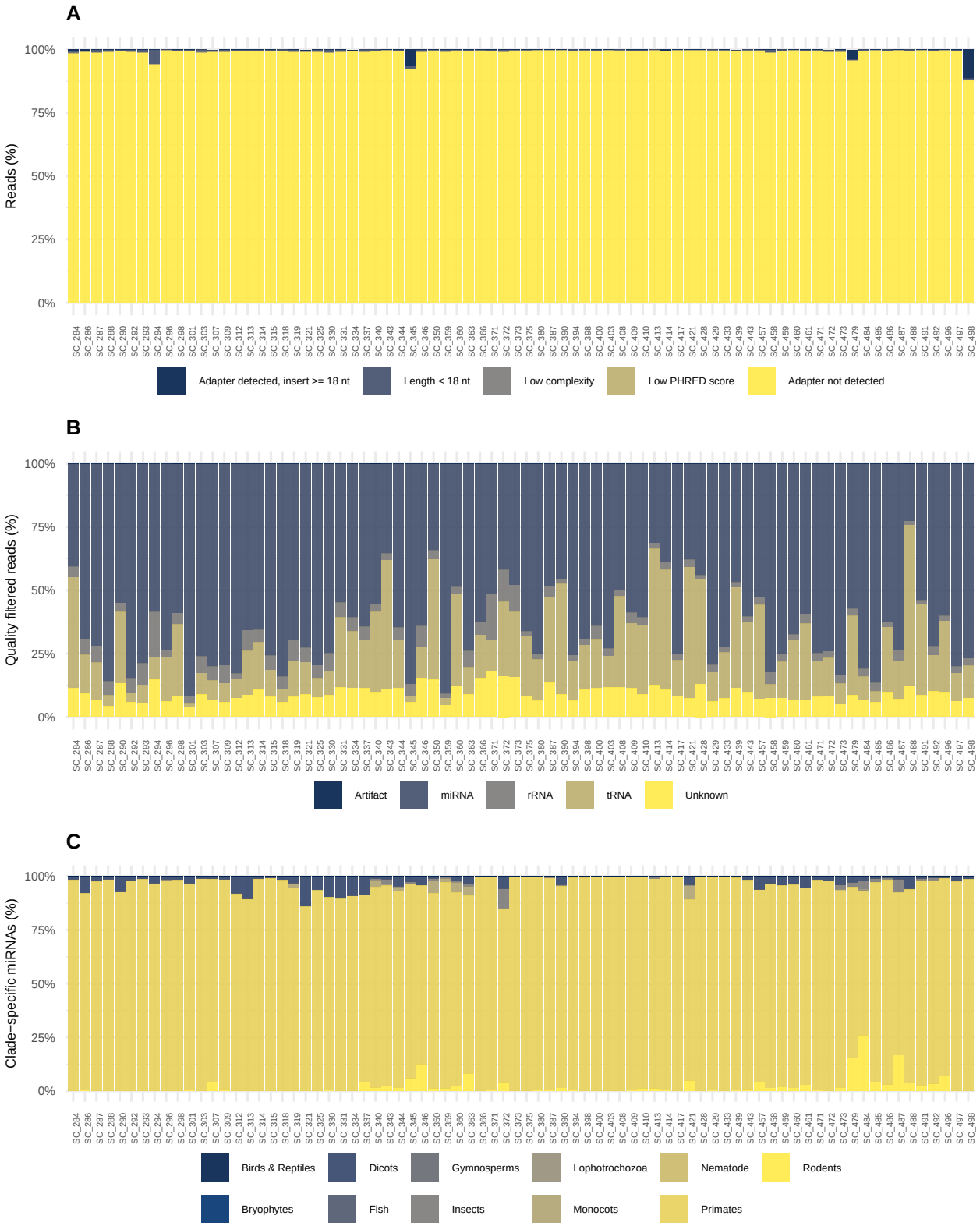

Figure 4.7: miRTrace (v1.0.1) Analysis. *A*: Quality control for small RNA sequencing data; *B*: RNA Categories; *C*: Contamination Check

In Figure 4.7 (A), the results of this analysis show that the adapters from the sequences of most samples have been successfully removed, with very few sequences measuring 18 nucleotides or more, indicating the presence of adapters; however, these sequences are not used in the subsequent analysis.. In the annotation step, the mapped reads against the databases indicate that more than 40% of the analyzed sequences per sample correspond to miRNA precursors Figure 4.7 (B).

In the contamination assessment step Figure 4.7 (C), sequences mapped against the specific clade miRNA catalog revealed that, in most samples, approximately 80% of the sequences belonged to the human category, although other clades such as Rodentia, Dicots, Insects, and Monocots were detected in low proportions. These identifications could result from contamination, such as incorrect index assignment during sample demultiplexing, or could have a biological origin.

The *nf-core/smrnaseq* pipeline includes the capability to perform differential expression analysis using *edgeR*. However, in this case, the differential expression analysis was conducted using the raw isomiR count files generated by *mirtop*. This approach was chosen because these files serve as foundational documents for subsequent analyses, enabling a more robust approach with specialized packages for isomiR analysis.

4.6 Differential expression analysis

The count matrix was obtained with the counts() function, which consolidates all isomiRs into a single feature: the reference miRNA. The table obtained is in the Appendix D.

For normalization, we used the *isomiRs* package, which applies the *rlog* transformation from the *DESeq2* package. This method facilitates quick integration into subsequent analyses, such as those shown in Figure 4.8. The figure shows a total of 374 reference miRNAs and demonstrates that no distinguishable groups are evident across all the samples when considering the conditions of sex and steatosis.

For pairwise comparisons, the likelihood ratio test (LRT) was used to identify miRNAs that show changes in expression across different levels. In this experiment, the goal is to identify miRNAs that are expressed differentially at various levels of steatosis.

With the LRT, the full model was compared to the reduced model to identify significant miRNAs. p-values were derived solely from the difference in deviance between the full and reduced model formulas, rather than from log2 fold changes. The threshold set for the padj was less than 0.05.

The number of significant miRNAs observed from the LRT is low Figure 4.9. In this model, a fold change criterion cannot be established, as the statistics are not generated from any pairwise comparisons. This list includes miRNAs that may be changing in any number of combinations across the four levels of steatosis. In the Table 4.4 shows the selected miRNAs.

In Figure 4.10, it can be seen that certain genes display extremely high dispersion values, highlighted with blue circles. This is likely because these genes deviate from the modeling assumptions and exhibit greater variability than others, potentially due to biological or technical factors.

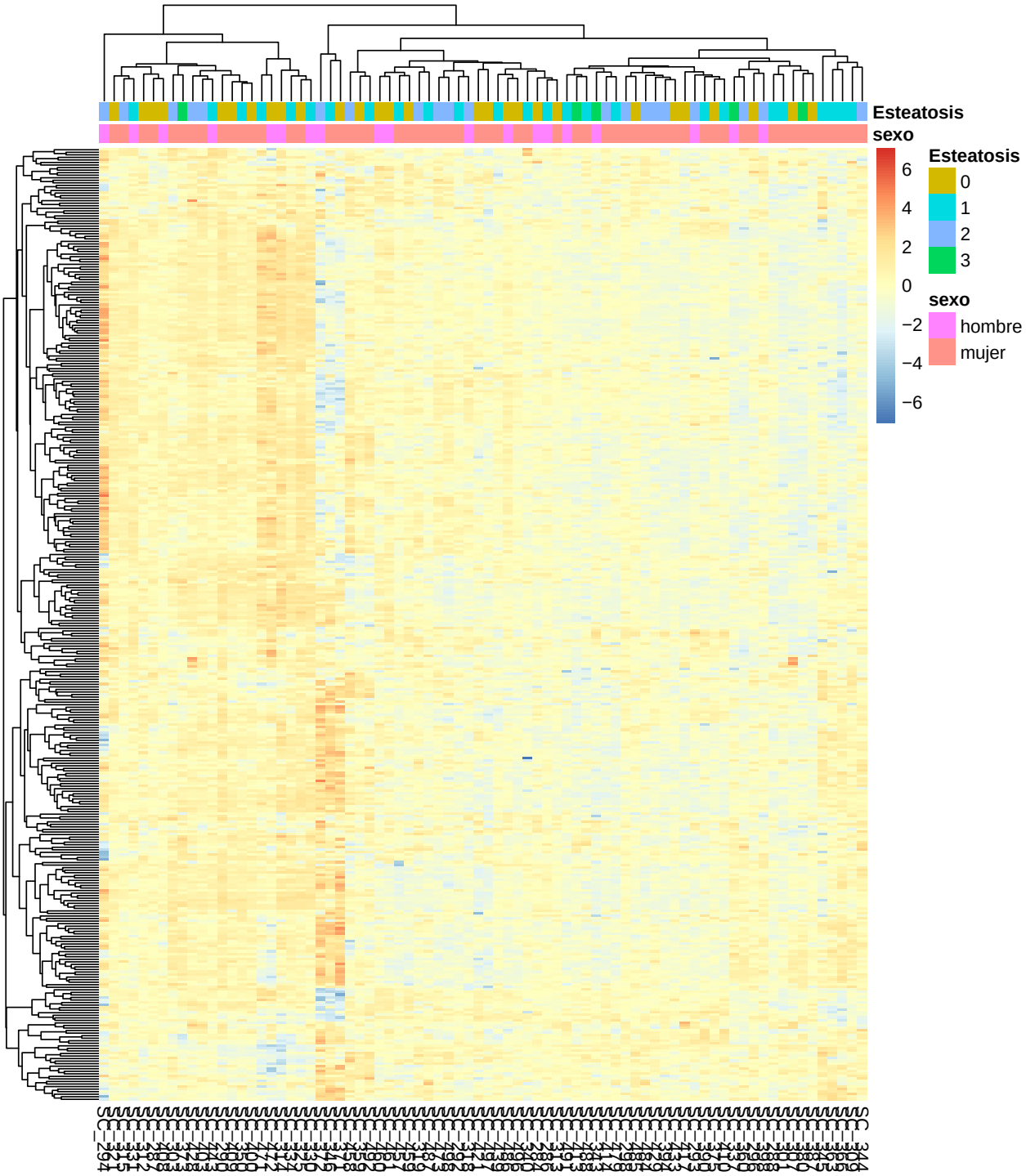

Figure 4.8: The heatmap displays all miRNA data (374) across all samples. In the heatmap, shades of red represent increased miRNA expression, while shades of blue signify reduced or absent miRNA expression. Despite the identification of numerous miRNAs, no clear grouping patterns were observed across the samples.

Table 4.4: Descriptive statistics of Isomir Read counts

miRNA reference	baseMean	log2FoldChange	lfcSE	stat	pvalue	padj
hsa-miR-144-3p	134.72661	-3.319167	0.7852957	19.70378	0.0001955	0.0400182
hsa-miR-372-3p	79.17045	1.085230	0.6468928	19.51419	0.0002140	0.0400182

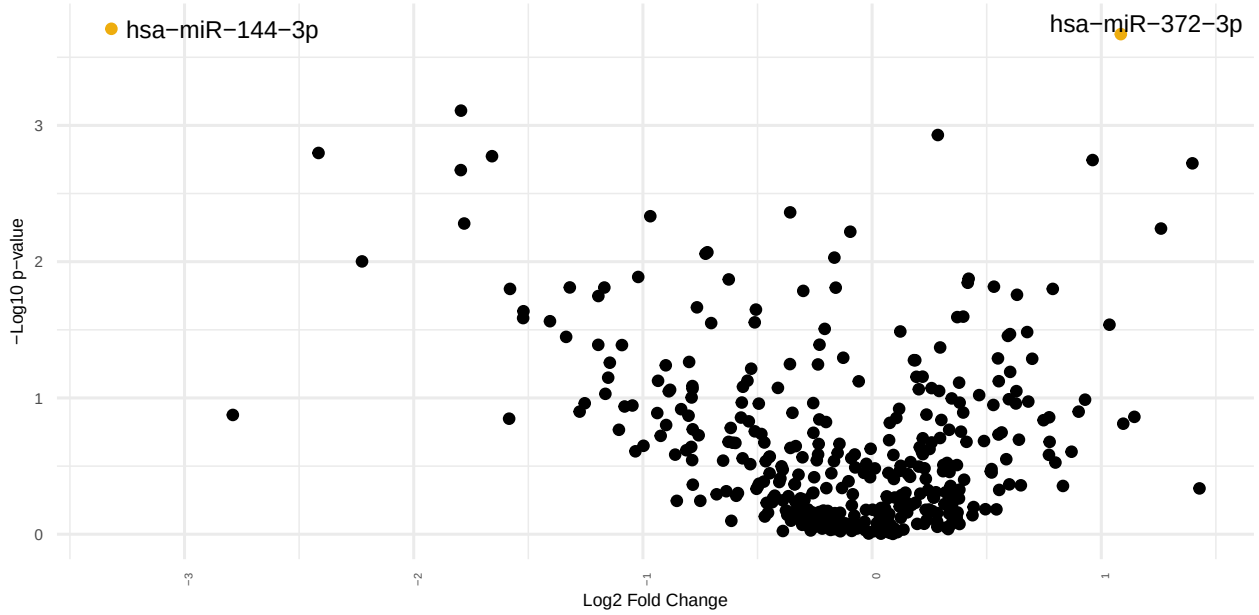

Figure 4.9: Volcano plot of DE miRNAs in the experiment.

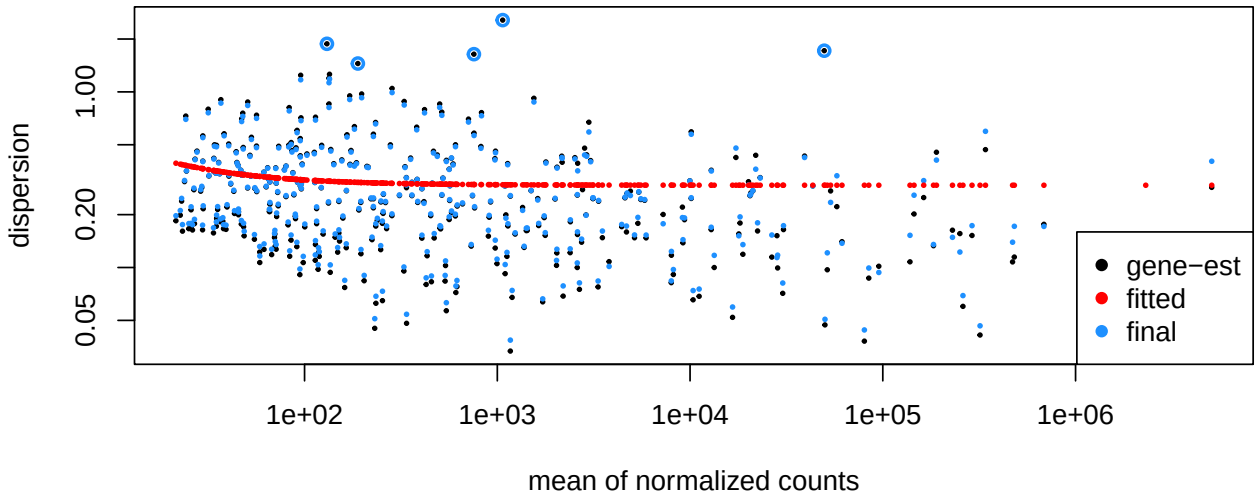

Figure 4.10: Estimation of the dispersion

In Figure 4.11, the selected miRNAs are shown. The miRNA *hsa-miR-144-3p* exhibits a decrease in expression as the level of steatosis increases, whereas *hsa-miR-372-3p* shows a trend of increasing expression across the different levels of steatosis.

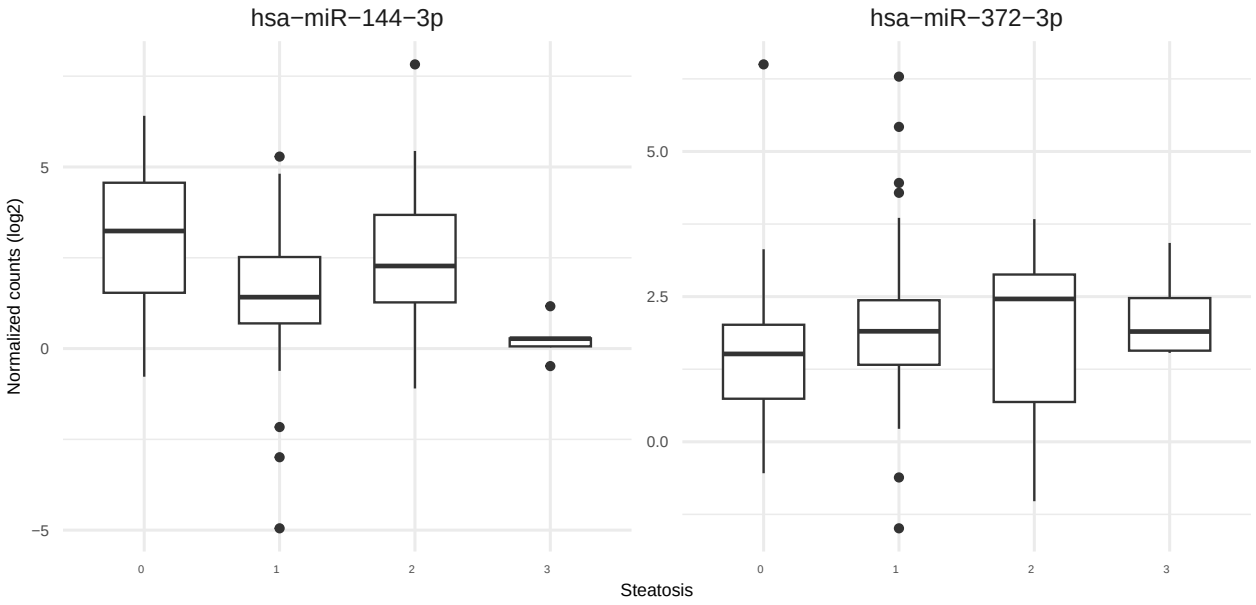

Figure 4.11: Steatosis levels of miRNAs selected

4.7 Target mRNA Selection and Validation

4.7.1 *hsa-miR-372-3p*

In Table 4.5, the target genes obtained by the *multiMiR* package after filtering are shown. These genes were used for the enrichment analysis of GO (Gene Ontology) categories, utilizing the clusterProfile library from Bioconductor (Xu et al., 2024). In Figure 4.12, the most represented GO categories for the target genes are observed, which relate to processes associated with developmental biology, cellular regulation, and neurobiology.

Table 4.5: Selected interactions after filtering by database, experiment type (including luciferase assays, Western blot, or qRT-PCR), functional support (Functional MTI) and validated type for *hsa-miR-372-3p*

database	mature_mirna_id	target_symbol	target_ensembl	pubmed_id	type
mirtarbase	hsa-miR-372-3p	LATS2	ENSG00000150457	18155131	validated
mirtarbase	hsa-miR-372-3p	LATS2	ENSG00000150457	20216554	validated
mirtarbase	hsa-miR-372-3p	LATS2	ENSG00000150457	16564011	validated
mirtarbase	hsa-miR-372-3p	LATS2	ENSG00000150457	22027184	validated
mirtarbase	hsa-miR-372-3p	LATS2	ENSG00000150457	19937137	validated
mirtarbase	hsa-miR-372-3p	TGFBR2	ENSG00000163513	21490602	validated
mirtarbase	hsa-miR-372-3p	TGFBR2	ENSG00000163513	22020335	validated
mirtarbase	hsa-miR-372-3p	NFIB	ENSG00000147862	21608007	validated
mirtarbase	hsa-miR-372-3p	CDKN1A	ENSG00000124762	18212054	validated
mirtarbase	hsa-miR-372-3p	CDKN1A	ENSG00000124762	20190813	validated
mirtarbase	hsa-miR-372-3p	VEGFA	ENSG00000112715	18320040	validated
mirtarbase	hsa-miR-372-3p	TNFAIP1	ENSG00000109079	23242208	validated
mirtarbase	hsa-miR-372-3p	TRPS1	ENSG00000104447	19229866	validated

mirtarbase	hsa-miR-372-3p	MBNL2	ENSG00000139793	19229866	validated
mirtarbase	hsa-miR-372-3p	RHOC	ENSG00000155366	21490602	validated
mirtarbase	hsa-miR-372-3p	NR4A2	ENSG00000153234	19885849	validated
mirtarbase	hsa-miR-372-3p	ERBB4	ENSG00000178568	19885849	validated
mirtarbase	hsa-miR-372-3p	CDK2	ENSG00000123374	21646351	validated
mirtarbase	hsa-miR-372-3p	CDK2	ENSG00000123374	23479742	validated
mirtarbase	hsa-miR-372-3p	LEFTY1	ENSG00000243709	22020335	validated
mirtarbase	hsa-miR-372-3p	BTG1	ENSG00000133639	22020335	validated
mirtarbase	hsa-miR-372-3p	CCNA1	ENSG00000133101	21646351	validated
mirtarbase	hsa-miR-372-3p	DKK1	ENSG00000107984	22020335	validated
mirtarbase	hsa-miR-372-3p	PHLPP2	ENSG00000040199	25160587	validated
mirtarbase	hsa-miR-372-3p	ATAD2	ENSG00000156802	24552534	validated
mirtarbase	hsa-miR-372-3p	TXNIP	ENSG00000265972	22660396	validated
mirtarbase	hsa-miR-372-3p	KLF13	ENSG00000275746	19229866	validated

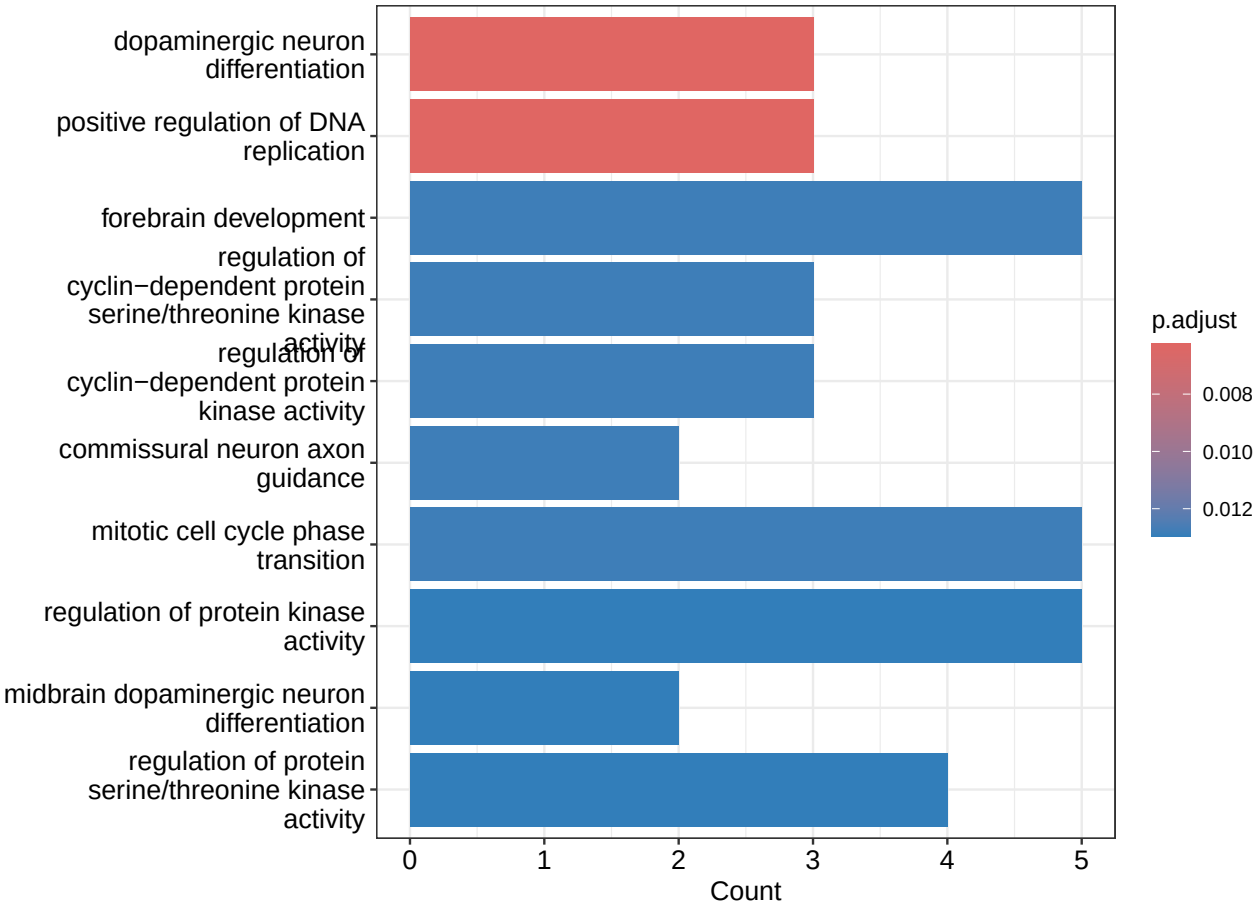

Figure 4.12: Top 10 Validated Enriched Biological Processes Enriquecidos of *hsa-miR-372-3p*

In Figure 4.13, two networks are displayed. The first illustrates the interactions between proteins involved in neurobiology, while the second shows the expression correlation among genes associated with cellular regulation. The absence of shared genes between both networks suggests that the biological processes they represent are distinct and do not interact directly.

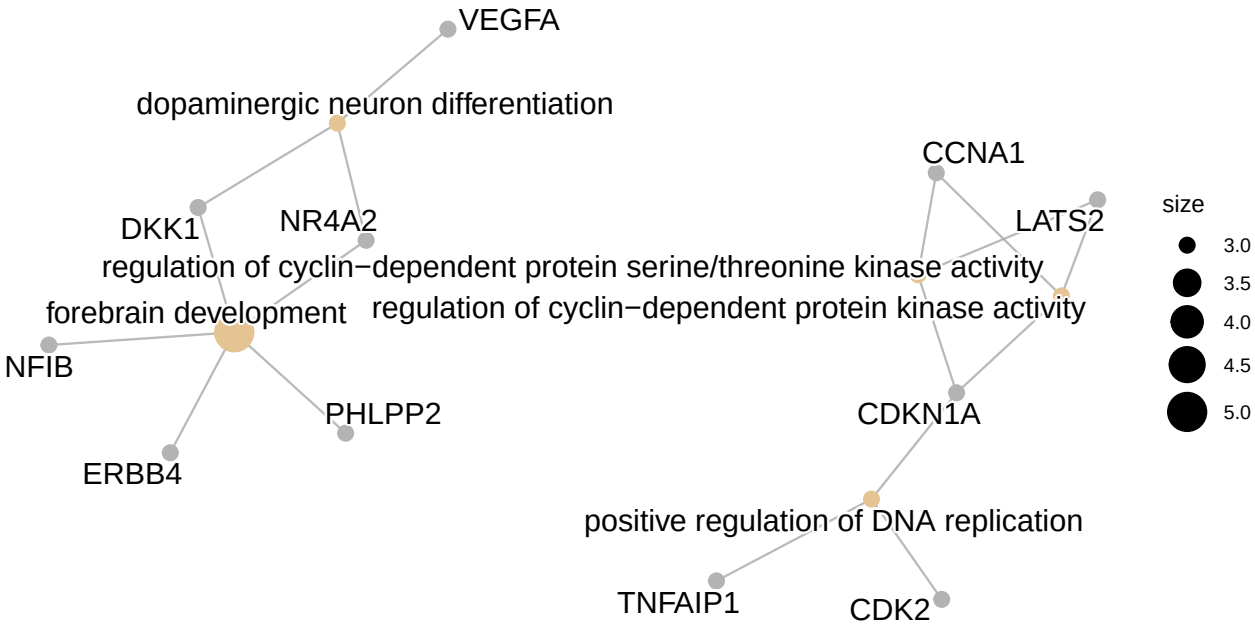

Figure 4.13: cnetplot of the target genes selected for *hsa-miR-372-3p*, in which the relationship between possible target genes and biological processes can be seen.

4.7.2 *hsa-miR-144-3p*

In Table 4.6, the target genes obtained by the *multiMiR* package after filtering are shown. These genes were used for the enrichment analysis of GO (Gene Ontology) categories, utilizing the clusterProfile library. In Figure 4.14, the most represented GO categories for the target genes are observed, which relate to processes associated with cell migration, cellular differentiation and developmental biology.

Table 4.6: Selected interactions after filtering by database, experiment type (including luciferase assays, Western blot, or qRT-PCR), functional support (Functional MTI) and validated type for *hsa-miR-144-3p*

database	mature_mirna_id	target_symbol	target_ensembl	pubmed_id	type
mirtarbase	hsa-miR-144-3p	NOTCH1	ENSG00000148400	21285251	validated
mirtarbase	hsa-miR-144-3p	NOTCH1	ENSG00000148400	21929751	validated
mirtarbase	hsa-miR-144-3p	PLAG1	ENSG00000181690	19347935	validated
mirtarbase	hsa-miR-144-3p	ZEB1	ENSG00000148516	27785072	validated
mirtarbase	hsa-miR-144-3p	ZEB2	ENSG00000169554	27785072	validated
mirtarbase	hsa-miR-144-3p	IRS1	ENSG00000169047	27069535	validated
mirtarbase	hsa-miR-144-3p	MAP3K8	ENSG00000107968	27717821	validated
mirtarbase	hsa-miR-144-3p	EZH2	ENSG00000106462	23815091	validated
mirtarbase	hsa-miR-144-3p	APP	ENSG00000142192	27329039	validated
mirtarbase	hsa-miR-144-3p	PTGS2	ENSG00000073756	26959737	validated
mirtarbase	hsa-miR-144-3p	MET	ENSG00000105976	25927670	validated
mirtarbase	hsa-miR-144-3p	MET	ENSG00000105976	26250785	validated
mirtarbase	hsa-miR-144-3p	ETS1	ENSG00000134954	26826553	validated
mirtarbase	hsa-miR-144-3p	TGFB1	ENSG00000105329	21991303	validated

mirtarbase	hsa-miR-144-3p	CFTR	ENSG00000001626	23226399	validated
mirtarbase	hsa-miR-144-3p	FGG	ENSG00000171557	20570858	validated
mirtarbase	hsa-miR-144-3p	MTOR	ENSG00000198793	22983984	validated
mirtarbase	hsa-miR-144-3p	MTOR	ENSG00000198793	26687302	validated
mirtarbase	hsa-miR-144-3p	MTOR	ENSG00000198793	27072960	validated
mirtarbase	hsa-miR-144-3p	SMAD4	ENSG00000141646	26918315	validated
mirtarbase	hsa-miR-144-3p	NFE2L2	ENSG00000116044	23236440	validated
mirtarbase	hsa-miR-144-3p	NFE2L2	ENSG00000116044	27508019	validated
mirtarbase	hsa-miR-144-3p	PBX3	ENSG00000167081	28111340	validated
mirtarbase	hsa-miR-144-3p	TTN	ENSG00000155657	24453045	validated
mirtarbase	hsa-miR-144-3p	TUG1	ENSG00000253352	27261864	validated
mirtarbase	hsa-miR-144-3p	PTEN	ENSG00000284792	23125220	validated
mirtarbase	hsa-miR-144-3p			25151965	validated
mirtarbase	hsa-miR-144-3p	XIST	ENSG00000229807	28059474	validated

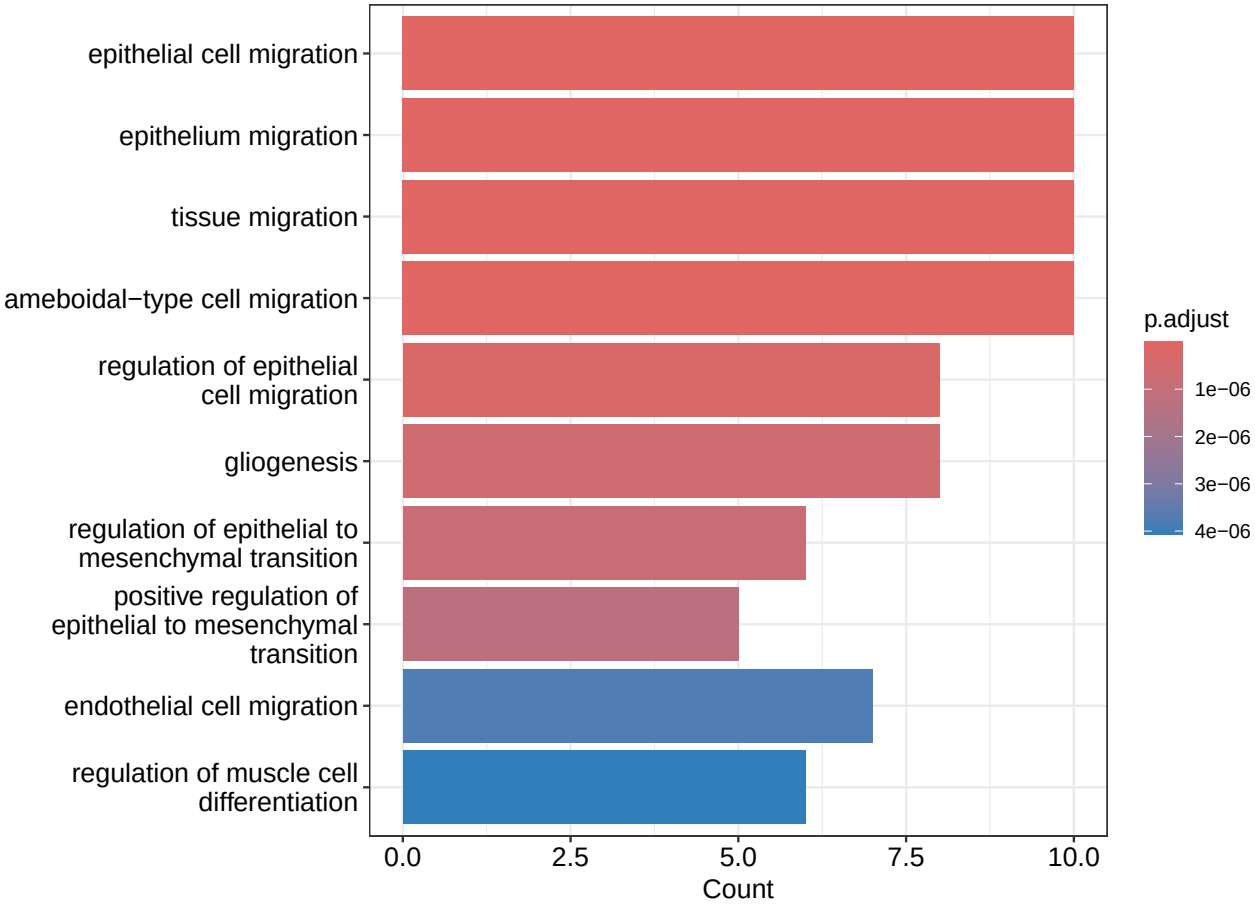

Figure 4.14: Top 10 Validated Enriched Biological Processes Enriquecidos of *hsa-miR-144-3p*

In Figure 4.15, network representing several processes related to cell migration, including epithelial cell migration, tissue migration and amoeboid-like migration. The inclusion of 'regulation of epithelial cell migration' indicates that there are regulatory mechanisms affecting all of these processes, suggesting a significant interconnection between them. This network highlights the

importance of cell migration in physiological processes such as tissue repair and its potential involvement in disease.

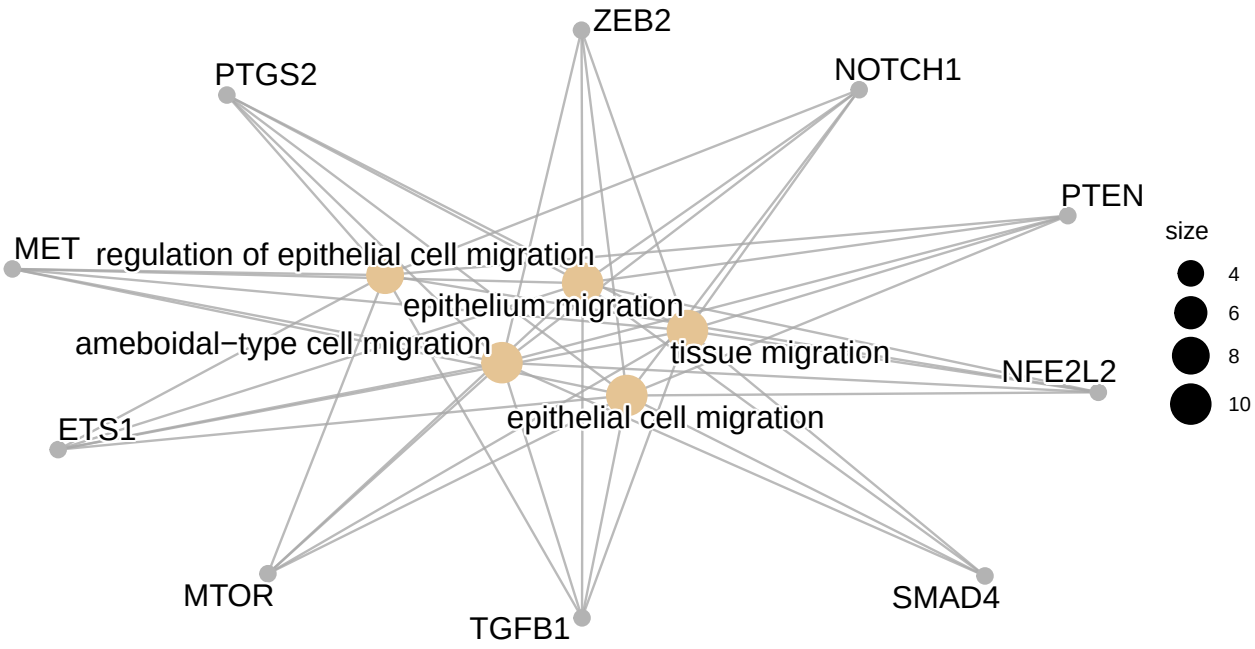

Figure 4.15: cnetplot of the target genes selected for *hsa-miR-144-3p,* in which the relationship between possible target genes and biological processes can be seen.

Chapter 5

Discussion

Chapter 6

Conclusions

Chapter 7

Recommendations

lalallallalalalallalala

Appendix A

Appendices

The following tables and figures present the alignment results using Samtools for all samples analyzed.

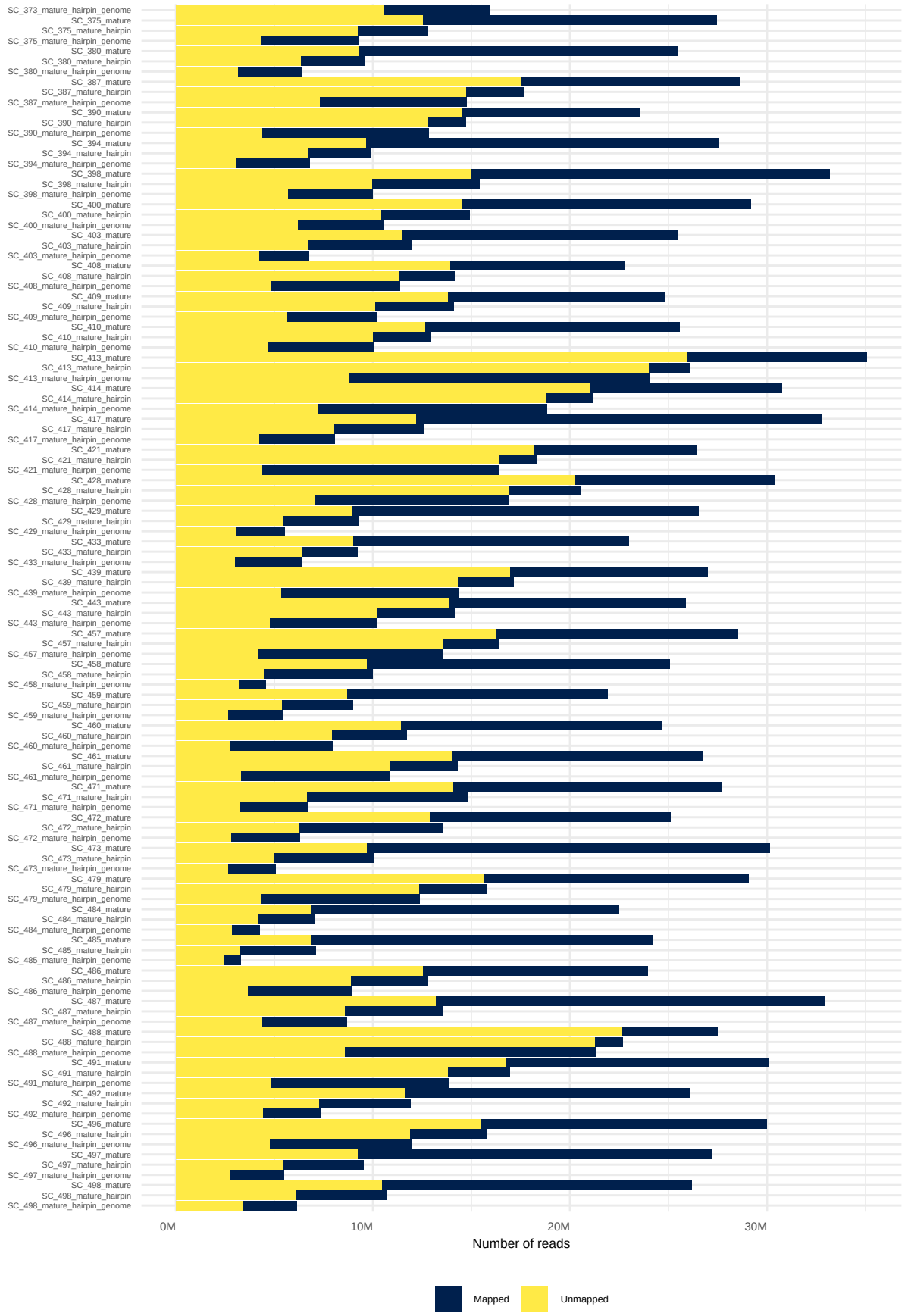

Figure A.1: Samtools: stats: Aligment Scores

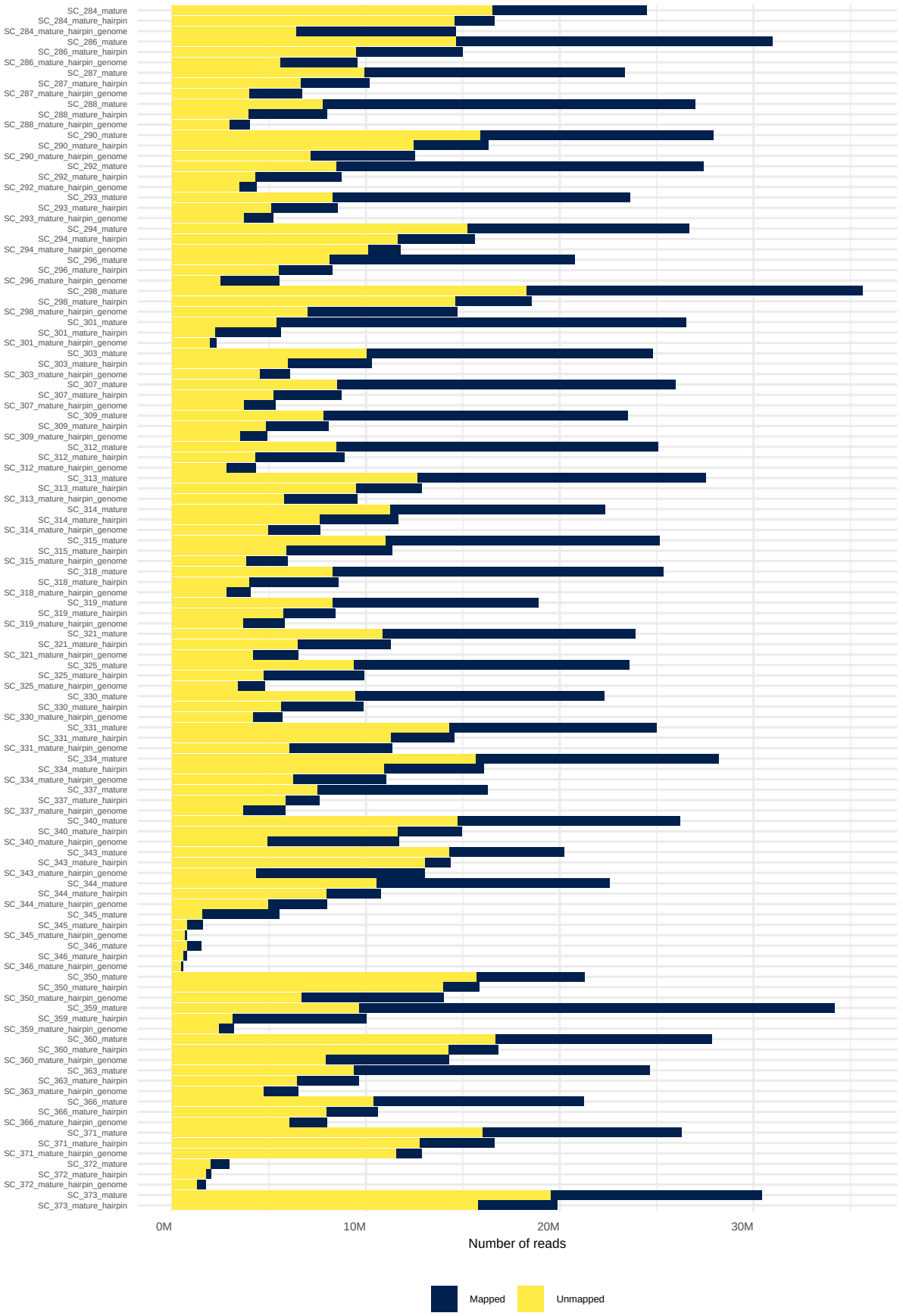

Figure A.2: Samtools: stats: Aligment Scores

Appendix B

Appendices

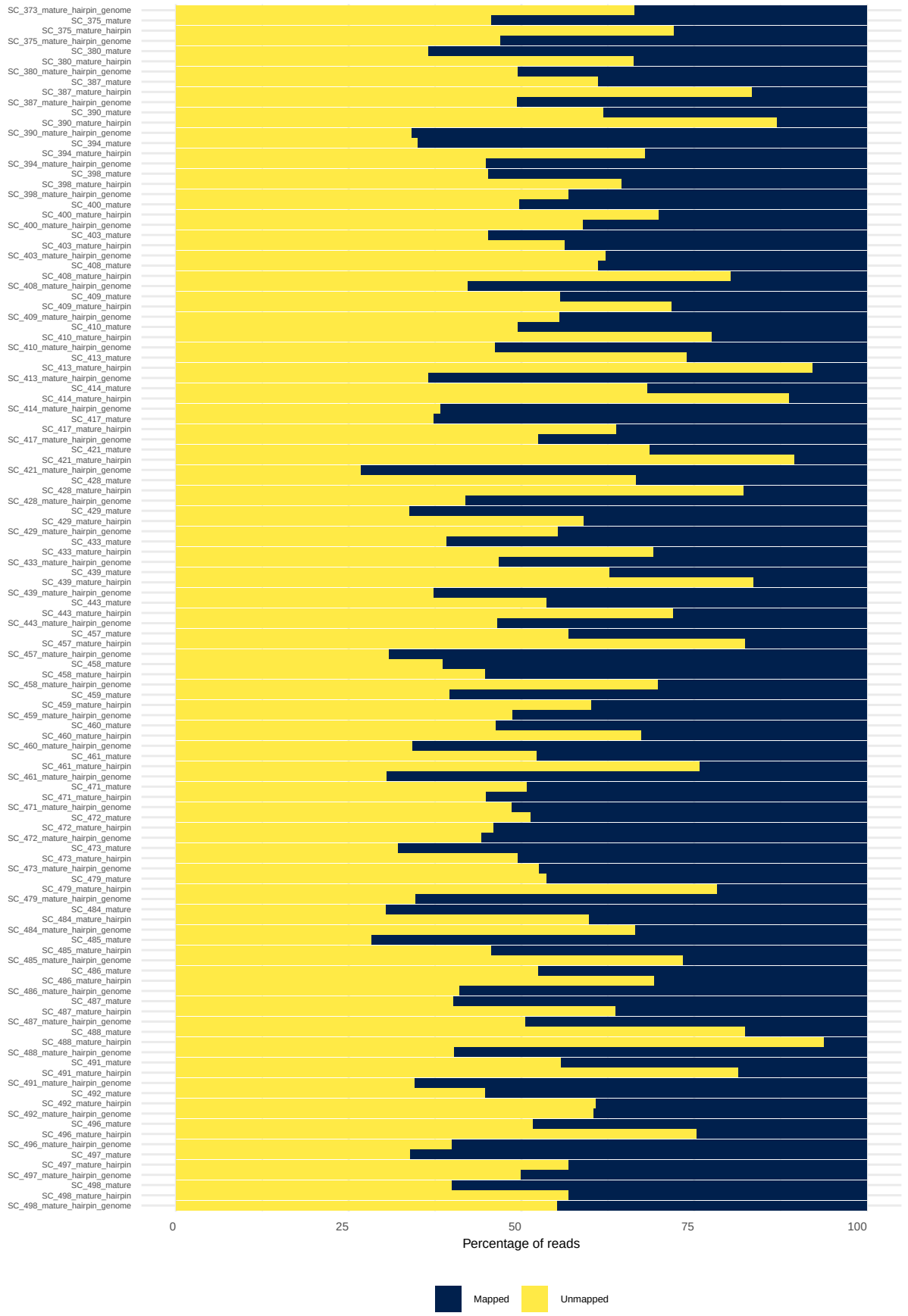

Figure B.1: Samtools: stats: Aligment Scores in percentages

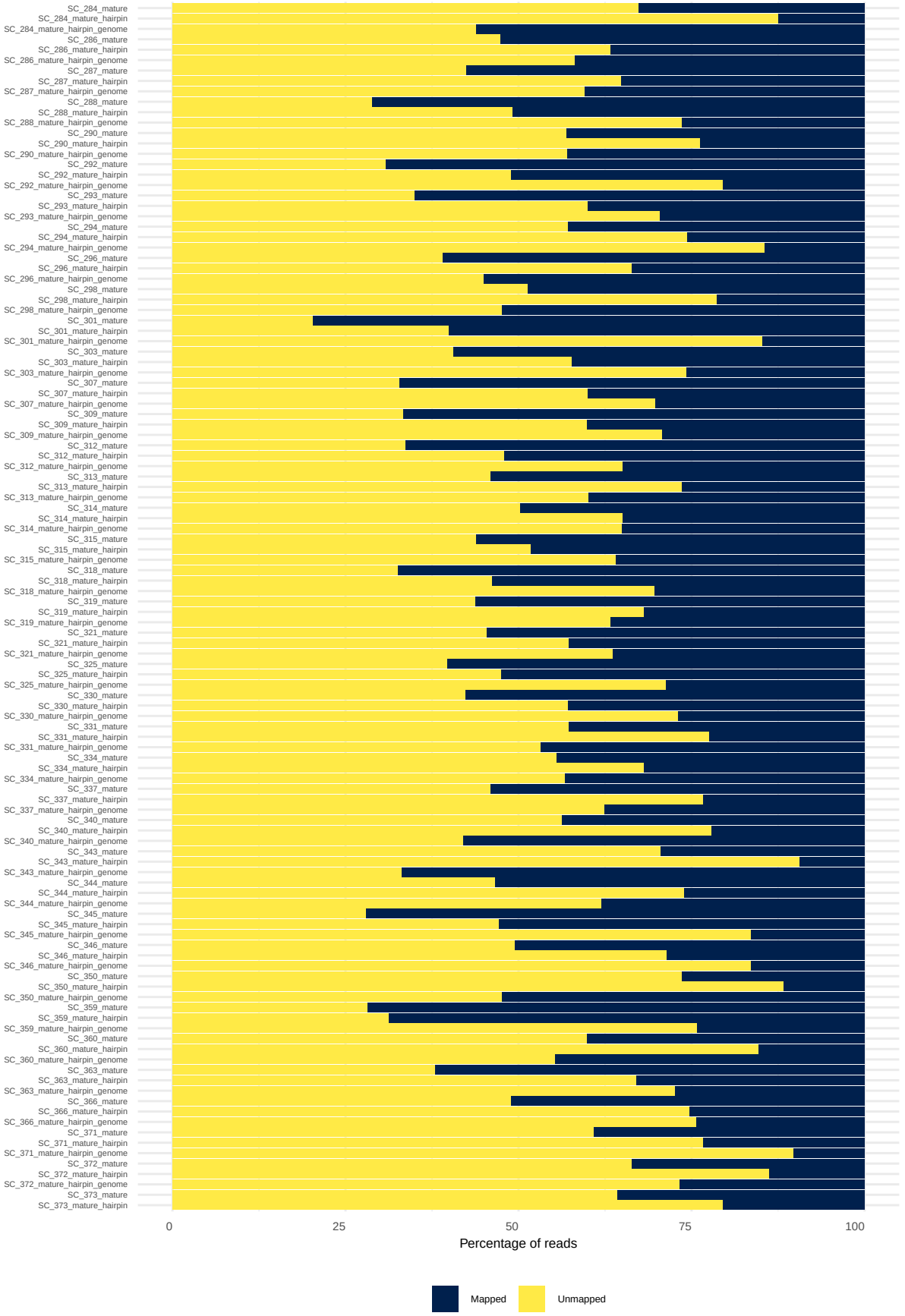

Figure B.2: Samtools: stats: Aligment Scores in percentages

Appendix C

Appendices

Table C.1: Alignment stats with Samtools (version 1.16.1)

Sample	Mapped reads	Unmapped reads	% Mapped	% Unmapped
SC_498_mature_hairpin_genome	2744597	3371428	44.875503	55.12450
SC_498_mature_hairpin	4617520	6060341	43.243867	56.75613
SC_498_mature	15766696	10440192	60.162412	39.83759
SC_497_mature_hairpin_genome	2735429	2724480	50.100267	49.89973
SC_497_mature_hairpin	4111775	5404453	43.208034	56.79197
SC_497_mature	18023058	9212014	66.175915	33.82409
SC_496_mature_hairpin_genome	7165355	4760107	60.084507	39.91549
SC_496_mature_hairpin	3903051	11870674	24.744003	75.25600
SC_496_mature	14490643	15486155	48.339529	51.66047
SC_492_mature_hairpin_genome	2893437	4415210	39.589229	60.41077
SC_492_mature_hairpin	4691937	7236935	39.332613	60.66739
SC_492_mature	14407144	11646032	55.298993	44.70101
SC_491_mature_hairpin_genome	9050120	4777210	65.450958	34.54904
SC_491_mature_hairpin	3153686	13788818	18.614049	81.38595
SC_491_mature	13351633	16738581	44.372011	55.62799
SC_488_mature_hairpin_genome	12744195	8553088	59.839534	40.16047
SC_488_mature_hairpin	1432302	21260358	6.311741	93.68826
SC_488_mature	4870620	22612182	17.722429	82.27757
SC_487_mature_hairpin_genome	4278599	4376546	49.434169	50.56583
SC_487_mature_hairpin	4927556	8578919	36.482917	63.51708
SC_487_mature	19747408	13190175	59.954029	40.04597
SC_486_mature_hairpin_genome	5248198	3638952	59.053780	40.94622
SC_486_mature_hairpin	3940979	8853917	30.801180	69.19882
SC_486_mature	11412197	12540551	47.644625	52.35537
SC_485_mature_hairpin_genome	876498	2405472	26.706460	73.29354
SC_485_mature_hairpin	3870100	3248134	54.368822	45.63118
SC_485_mature	17333731	6838753	71.708522	28.29148
SC_484_mature_hairpin_genome	1432239	2829136	33.609786	66.39021
SC_484_mature_hairpin	2820206	4190029	40.229835	59.77016
SC_484_mature	15650928	6831574	69.613818	30.38618
SC_479_mature_hairpin_genome	8108405	4281557	65.443340	34.55666
SC_479_mature_hairpin	3431530	12337417	21.761313	78.23869
SC_479_mature	13487647	15581922	46.397822	53.60218

SC_473_mature_hairpin_genome	2392675	2642806	47.516315	52.48369
SC_473_mature_hairpin	5073951	4948371	50.626502	49.37350
SC_473_mature	20467672	9676396	67.899502	32.10050
SC_472_mature_hairpin_genome	3511799	2775384	55.856478	44.14352
SC_472_mature_hairpin	7331665	6217497	54.111575	45.88842
SC_472_mature	12218247	12885627	48.670763	51.32924
SC_471_mature_hairpin_genome	3453391	3254426	51.483083	48.51692
SC_471_mature_hairpin	8164995	6641090	55.146212	44.85379
SC_471_mature	13664246	14052468	49.299661	50.70034
SC_461_mature_hairpin_genome	7563990	3304204	69.597488	30.40251
SC_461_mature_hairpin	3469039	10813155	24.289258	75.71074
SC_461_mature	12790056	13974337	47.787581	52.21242
SC_460_mature_hairpin_genome	5230030	2708863	65.878580	34.12142
SC_460_mature_hairpin	3835718	7903166	32.675321	67.32468
SC_460_mature	13237348	11399583	53.729695	46.27030
SC_459_mature_hairpin_genome	2783611	2639003	51.333379	48.66662
SC_459_mature_hairpin	3582548	5378163	39.980622	60.01938
SC_459_mature	13242432	8680672	60.404001	39.59600
SC_458_mature_hairpin_genome	1375038	3171515	30.243527	69.75647
SC_458_mature_hairpin	5505378	4459196	55.249507	44.75049
SC_458_mature	15408741	9676346	61.425902	38.57410
SC_457_mature_hairpin_genome	9385631	4177300	69.200610	30.79939
SC_457_mature_hairpin	2909240	13515507	17.712541	82.28746
SC_457_mature	12335871	16210908	43.212830	56.78717
SC_443_mature_hairpin_genome	5468937	4747805	53.529168	46.47083
SC_443_mature_hairpin	3974281	10179572	28.079146	71.92085
SC_443_mature	12034498	13864526	46.466994	53.53301
SC_439_mature_hairpin_genome	9000706	5346326	62.735666	37.26433
SC_439_mature_hairpin	2826157	14310067	16.492297	83.50770
SC_439_mature	10058851	16933174	37.266011	62.73399
SC_433_mature_hairpin_genome	3412034	2991006	53.287720	46.71228
SC_433_mature_hairpin	2852106	6362163	30.953145	69.04686
SC_433_mature	13979932	8989589	60.862967	39.13703
SC_429_mature_hairpin_genome	2465541	3040548	44.778444	55.22156
SC_429_mature_hairpin	3799870	5450107	41.079778	58.92022
SC_429_mature	17580501	8947853	66.270606	33.72939
SC_428_mature_hairpin_genome	9835883	7078888	58.149667	41.85033
SC_428_mature_hairpin	3667182	16868667	17.857465	82.14254
SC_428_mature	10167817	20226533	33.452984	66.54702
SC_421_mature_hairpin_genome	12039297	4382042	73.314953	26.68505
SC_421_mature_hairpin	1921054	16367524	10.504119	89.49588
SC_421_mature	8334983	18125108	31.500205	68.49979
SC_417_mature_hairpin_genome	3840665	4230821	47.583122	52.41688
SC_417_mature_hairpin	4558184	8009437	36.269267	63.73073
SC_417_mature	20566865	12189260	62.787845	37.21216
SC_414_mature_hairpin_genome	11626154	7192202	61.780923	38.21908
SC_414_mature_hairpin	2384522	18764466	11.274875	88.72512
SC_414_mature	9773314	20975321	31.784546	68.21545
SC_413_mature_hairpin_genome	15273686	8755282	63.563637	36.43636
SC_413_mature_hairpin	2075044	23986778	7.962007	92.03799
SC_413_mature	9149532	25922290	26.087986	73.91201
SC_410_mature_hairpin_genome	5421609	4646857	53.847418	46.15258
SC_410_mature_hairpin	2900623	9994884	22.493284	77.50672

SC_410_mature	12919955	12648790	50.530267	49.46973
SC_409_mature_hairpin_genome	4530560	5646158	44.518871	55.48113
SC_409_mature_hairpin	3999053	10117341	28.329140	71.67086
SC_409_mature	11038048	13776426	44.482297	55.51770
SC_408_mature_hairpin_genome	6583428	4797782	57.844711	42.15529
SC_408_mature_hairpin	2790714	11336814	19.753732	80.24627
SC_408_mature	8876025	13926824	38.925070	61.07493
SC_403_mature_hairpin_genome	2558149	4200888	37.847833	62.15217
SC_403_mature_hairpin	5223502	6717196	43.745366	56.25463
SC_403_mature	13969652	11492819	54.863693	45.13631
SC_400_mature_hairpin_genome	4330659	6183592	41.188469	58.81153
SC_400_mature_hairpin	4497625	10417103	30.155595	69.84440
SC_400_mature	14697933	14468745	50.392894	49.60711
SC_398_mature_hairpin_genome	4324574	5666444	43.284618	56.71538
SC_398_mature_hairpin	5469763	9937686	35.500770	64.49923
SC_398_mature	18207151	14977889	54.865539	45.13446
SC_394_mature_hairpin_genome	3740196	3041386	55.152264	44.84774
SC_394_mature_hairpin	3180039	6725726	32.102912	67.89709
SC_394_mature	17895589	9632687	65.008027	34.99197
SC_390_mature_hairpin_genome	8452470	4373750	65.899930	34.10007
SC_390_mature_hairpin	1923806	12776493	13.086849	86.91315
SC_390_mature	8992467	14532067	38.225909	61.77409
SC_387_mature_hairpin_genome	7490021	7285833	50.690952	49.30905
SC_387_mature_hairpin	2952557	14726708	16.700677	83.29932
SC_387_mature	11167772	17470973	38.995326	61.00467
SC_380_mature_hairpin_genome	3221221	3148514	50.570722	49.42928
SC_380_mature_hairpin	3235044	6323416	33.844824	66.15518
SC_380_mature	16180366	9298625	63.504736	36.49526
SC_375_mature_hairpin_genome	4917429	4347342	53.076638	46.92336
SC_375_mature_hairpin	3585422	9209182	28.022923	71.97708
SC_375_mature	14945565	12507898	54.439635	45.56037
SC_373_mature_hairpin_genome	5364365	10568678	33.668176	66.33182
SC_373_mature_hairpin	4069070	15784794	20.495104	79.50490
SC_373_mature	10899376	19530932	35.817501	64.18250
SC_372_mature_hairpin_genome	466361	1277379	26.744870	73.25513
SC_372_mature_hairpin	278775	1729919	13.878421	86.12158
SC_372_mature	1000037	1972216	33.645756	66.35424
SC_371_mature_hairpin_genome	1323766	11554287	10.279240	89.72076
SC_371_mature_hairpin	3884222	12742372	23.361501	76.63850
SC_371_mature	10311186	15986343	39.209714	60.79029
SC_366_mature_hairpin_genome	1950351	6049547	24.379698	75.62030
SC_366_mature_hairpin	2692286	7946340	25.306708	74.69329
SC_366_mature	10855919	10385584	51.107113	48.89289
SC_363_mature_hairpin_genome	1785360	4719578	27.446226	72.55377
SC_363_mature_hairpin	3172307	6443801	32.989511	67.01049
SC_363_mature	15283542	9347917	62.048870	37.95113
SC_360_mature_hairpin_genome	6393637	7899608	44.731879	55.26812
SC_360_mature_hairpin	2586814	14249692	15.364316	84.63568
SC_360_mature	11191408	16650498	40.196271	59.80373
SC_359_mature_hairpin_genome	772978	2413120	24.260961	75.73904
SC_359_mature_hairpin	6897759	3123516	68.831152	31.16885
SC_359_mature	24559803	9623594	71.847169	28.15283
SC_350_mature_hairpin_genome	7348569	6670062	52.420019	47.57998
SC_350_mature_hairpin	1865905	13978181	11.776665	88.22333

SC_350_mature	5626041	15675998	26.410810	73.58919
SC_346_mature_hairpin_genome	91722	465433	16.462564	83.53744
SC_346_mature_hairpin	220717	550982	28.601437	71.39856
SC_346_mature	770483	751722	50.616244	49.38376
SC_345_mature_hairpin_genome	127582	648916	16.430435	83.56956
SC_345_mature_hairpin	849937	757561	52.873285	47.12671
SC_345_mature	3988391	1545899	72.066896	27.93310
SC_344_mature_hairpin_genome	3046790	4962062	38.042781	61.95722
SC_344_mature_hairpin	2812683	7958051	26.114126	73.88587
SC_344_mature	12059312	10526656	53.392938	46.60706
SC_343_mature_hairpin_genome	8740107	4309858	66.974180	33.02582
SC_343_mature_hairpin	1363224	13018072	9.479146	90.52085
SC_343_mature	5966144	14278700	29.469943	70.53006
SC_340_mature_hairpin_genome	6785632	4908122	58.027833	41.97217
SC_340_mature_hairpin	3322263	11635484	22.210985	77.78901
SC_340_mature	11452686	14734344	43.734192	56.26581
SC_337_mature_hairpin_genome	2208061	3653634	37.669326	62.33067
SC_337_mature_hairpin	1772336	5826603	23.323467	76.67653
SC_337_mature	8812419	7468275	54.128030	45.87197
SC_334_mature_hairpin_genome	4784762	6247131	43.372085	56.62792
SC_334_mature_hairpin	5136883	10932584	31.966729	68.03327
SC_334_mature	12556898	15637192	44.537341	55.46266
SC_331_mature_hairpin_genome	5319405	6041206	46.823230	53.17677
SC_331_mature_hairpin	3271056	11288070	22.467393	77.53261
SC_331_mature	10694971	14296881	42.793831	57.20617
SC_330_mature_hairpin_genome	1533651	4154713	26.961197	73.03880
SC_330_mature_hairpin	4228162	5616625	42.948232	57.05177
SC_330_mature	12882718	9425175	57.749596	42.25040
SC_325_mature_hairpin_genome	1372170	3391845	28.802806	71.19719
SC_325_mature_hairpin	5215807	4702310	52.588682	47.41132
SC_325_mature	14224823	9368454	60.291849	39.70815
SC_321_mature_hairpin_genome	2377820	4148758	36.432875	63.56713
SC_321_mature_hairpin	4819712	6455622	42.745625	57.25437
SC_321_mature	13052914	10840388	54.630013	45.36999
SC_319_mature_hairpin_genome	2131379	3668909	36.746089	63.25391
SC_319_mature_hairpin	2694449	5735368	31.963316	68.03668
SC_319_mature	10635070	8258957	56.288000	43.71200
SC_318_mature_hairpin_genome	1221577	2801202	30.366495	69.63350
SC_318_mature_hairpin	4627372	3959025	53.891894	46.10811
SC_318_mature	17082695	8248130	67.438368	32.56163
SC_315_mature_hairpin_genome	2138741	3809122	35.958142	64.04186
SC_315_mature_hairpin	5488459	5874581	48.300974	51.69903
SC_315_mature	14134369	11010585	56.211552	43.78845
SC_314_mature_hairpin_genome	2679436	4960119	35.073195	64.92681
SC_314_mature_hairpin	4087514	7583152	35.023828	64.97617
SC_314_mature	11126072	11233287	49.760246	50.23975
SC_313_mature_hairpin_genome	3825743	5754935	39.931861	60.06814
SC_313_mature_hairpin	3405941	9473724	26.444329	73.55567
SC_313_mature	14897240	12645169	54.088370	45.91163
SC_312_mature_hairpin_genome	1507700	2794434	35.045398	64.95460
SC_312_mature_hairpin	4644281	4260306	52.156052	47.84395
SC_312_mature	16636872	8446482	66.326345	33.67365
SC_309_mature_hairpin_genome	1441141	3483122	29.266126	70.73387
SC_309_mature_hairpin	3241007	4840223	40.105368	59.89463

SC_309_mature	15686563	7816291	66.743226	33.25677
SC_307_mature_hairpin_genome	1610746	3703775	30.308395	69.69161
SC_307_mature_hairpin	3494741	5227099	40.068850	59.93115
SC_307_mature	17469805	8501677	67.265337	32.73466
SC_303_mature_hairpin_genome	1565736	4501527	25.806299	74.19370
SC_303_mature_hairpin	4359563	5942747	42.316364	57.68364
SC_303_mature	14743705	10033956	59.504023	40.49598
SC_301_mature_hairpin_genome	338174	1945224	14.810121	85.18988
SC_301_mature_hairpin	3363956	2227328	60.164284	39.83572
SC_301_mature	21145107	5369457	79.749028	20.25097
SC_298_mature_hairpin_genome	7712913	6981737	52.487899	47.51210
SC_298_mature_hairpin	3975972	14579438	21.427562	78.57244
SC_298_mature	17360005	18269021	48.724332	51.27567
SC_296_mature_hairpin_genome	3048365	2484878	55.091833	44.90817
SC_296_mature_hairpin	2785017	5476804	33.709481	66.29052
SC_296_mature	12678516	8099488	61.018931	38.98107
SC_294_mature_hairpin_genome	1712011	10084572	14.512770	85.48723
SC_294_mature_hairpin	4005534	11624574	25.627040	74.37296
SC_294_mature	11423661	15233093	42.854659	57.14534
SC_293_mature_hairpin_genome	1549409	3678267	29.638581	70.36142
SC_293_mature_hairpin	3421304	5114103	40.083666	59.91633
SC_293_mature	15368091	8246741	65.078130	34.92187
SC_292_mature_hairpin_genome	895545	3466828	20.528850	79.47115
SC_292_mature_hairpin	4472883	4279211	51.106432	48.89357
SC_292_mature	18956815	8442108	69.188176	30.81182
SC_290_mature_hairpin_genome	5386944	7134399	43.022094	56.97791
SC_290_mature_hairpin	3892693	12447347	23.823032	76.17697
SC_290_mature	12024349	15894369	43.069130	56.93087
SC_288_mature_hairpin_genome	1061454	2947261	26.478660	73.52134
SC_288_mature_hairpin	4069560	3918737	50.944025	49.05598
SC_288_mature	19216109	7764252	71.222579	28.77742
SC_287_mature_hairpin_genome	2708510	3975337	40.523220	59.47678
SC_287_mature_hairpin	3584600	6605372	35.177722	64.82228
SC_287_mature	13471280	9895071	57.652476	42.34752
SC_286_mature_hairpin_genome	4007433	5551495	41.923456	58.07654
SC_286_mature_hairpin	5515837	9474968	36.794802	63.20520
SC_286_mature	16329833	14653293	52.705570	47.29443
SC_284_mature_hairpin_genome	8218701	6404276	56.204021	43.79598
SC_284_mature_hairpin	2085590	14554741	12.533344	87.46666
SC_284_mature	8003734	16508641	32.651809	67.34819

Appendix D

Appendices

	SC_284	SC_286	SC_287	SC_288	SC_290	SC_292	SC_293	SC_294	SC_296	SC_298	SC_3
hsa-let-7a-3p	163	456	471	211	1393	272	246	816	462	490	2
hsa-let-7a-5p	50531	139256	172089	75244	339094	105326	145709	7236	101678	201549	988
hsa-let-7b-3p	247	695	383	338	858	192	164	920	497	512	2
hsa-let-7b-5p	36029	84414	85389	59755	120574	113982	94565	24072	64982	112049	916
hsa-let-7c-3p	8	18	37	12	93	14	16	133	61	25	
hsa-let-7c-5p	17701	54923	46016	42478	58467	69723	53428	5804	42578	65171	637
hsa-let-7d-3p	341	820	416	419	1163	375	268	942	540	906	3
hsa-let-7d-5p	1130	2383	2516	1499	6601	2469	2358	1653	1528	3595	18
hsa-let-7e-3p	8	70	55	30	92	51	19	112	70	66	
hsa-let-7e-5p	3093	10087	9187	8606	14686	7252	7209	1350	6432	12965	82
hsa-let-7f-1-3p	95	218	141	167	120	90	155	382	199	181	1
hsa-let-7f-2-3p	12	80	61	63	106	83	81	683	21	88	
hsa-let-7f-5p	233603	527052	560208	380498	859237	522600	619996	29949	327858	649438	3869
hsa-let-7g-5p	73364	177764	205688	97774	354381	157688	183161	23644	105164	221257	1082
hsa-let-7i-3p	30	83	57	57	64	57	64	315	26	39	
hsa-let-7i-5p	307890	555123	568595	413470	652355	647959	689277	182244	385802	640559	4921
hsa-miR-1-3p	9617	11684	5402	14584	31249	12217	1108402	944	3531	98698	62
hsa-miR-100-5p	40385	137726	131332	108447	152661	89772	107773	135828	118370	73903	1602
hsa-miR-101-3p	40147	61182	79486	89923	57350	84725	71769	184442	24305	50691	313
hsa-miR-10395-3p	148	85	137	93	119	65	104	60	94	115	
hsa-miR-10399-3p	85	109	73	136	103	101	96	244	111	161	2
hsa-miR-10399-5p	7	13	27	11	35	11	29	30	14	30	
hsa-miR-103a-3p	18976	49935	42504	26500	68793	35036	30971	78572	24556	41560	226
hsa-miR-106a-5p	21	72	65	33	80	49	49	62	10	43	
hsa-miR-106b-3p	5328	9744	7516	10395	7294	8456	7963	6193	5999	9108	141
hsa-miR-106b-5p	396	690	776	833	543	1306	858	4764	322	637	4
hsa-miR-10a-3p	93	269	362	150	697	242	140	1173	118	282	2
hsa-miR-10a-5p	137255	369605	191931	184399	364243	196239	184213	253125	230482	186333	3099
hsa-miR-10b-3p	55	193	213	87	437	166	93	511	108	193	
hsa-miR-10b-5p	365764	1061811	403610	583854	626334	688835	444001	209239	615362	555078	7804
hsa-miR-1180-3p	99	151	139	118	123	209	136	82	120	208	1
hsa-miR-12136	11	12	31	37	43	72	27	255	4	70	
hsa-miR-122-5p	978	1188	778	1056	8766	2394	1211	928	1304	1033	13
hsa-miR-1246	173	151	256	98	117	113	687	13	42	280	
hsa-miR-1247-3p	15	28	47	51	35	48	44	24	139	30	
hsa-miR-1255a	18	14	41	31	78	35	27	21	17	34	

hsa-miR-125a-3p	20	60	78	63	152	40	44	19	55	134	
hsa-miR-125a-5p	1903	5892	5510	2758	18701	4117	2161	17862	3329	3771	29
hsa-miR-125b-1-3p	196	442	671	403	701	437	463	268	478	599	4
hsa-miR-125b-2-3p	735	1888	1614	2061	1640	1769	975	2730	1067	2068	15
hsa-miR-125b-5p	3595	14943	14157	6923	25515	12270	7766	21989	8117	9528	95
hsa-miR-126-3p	176478	303918	403417	360908	596384	444111	262537	851331	235002	484900	2772
hsa-miR-126-5p	770	1758	2556	1755	4366	2369	1251	8344	1206	2534	8
hsa-miR-127-3p	3383	13890	5865	12145	12650	11203	7082	7974	13585	14944	231
hsa-miR-127-5p	57	231	79	455	76	299	133	833	133	236	1
hsa-miR-1271-5p	40	129	119	94	314	100	62	408	57	186	1
hsa-miR-1278	10	34	36	46	87	26	30	32	11	31	
hsa-miR-128-1-5p	28	61	39	27	41	43	35	50	71	27	
hsa-miR-128-3p	1020	3243	3317	2933	4949	3466	1896	4217	2828	4483	39
hsa-miR-1287-5p	98	194	204	185	283	173	109	657	160	242	1
hsa-miR-129-5p	7	29	12	42	34	14	34	16	19	52	
hsa-miR-1290	31	19	52	75	49	89	70	35	18	86	
hsa-miR-1291	10	56	40	16	44	38	28	131	19	26	
hsa-miR-1296-5p	28	91	51	58	82	113	52	231	26	113	
hsa-miR-1299	87	521	230	366	307	2302	765	2	997	44	
hsa-miR-1301-3p	27	90	70	58	169	69	39	118	73	109	
hsa-miR-1303	44	85	131	78	448	87	73	430	53	186	
hsa-miR-1304-3p	15	29	28	30	44	39	37	26	15	23	
hsa-miR-1307-3p	252	675	901	579	1453	336	271	654	440	635	4
hsa-miR-130a-3p	45	122	148	136	197	192	114	387	96	117	
hsa-miR-130a-5p	11	35	26	37	11	61	29	4	26	60	
hsa-miR-132-3p	643	1251	732	821	1134	798	588	1401	835	921	5
hsa-miR-132-5p	102	220	182	196	172	248	144	415	252	223	2
hsa-miR-133a-3p	35	160	37	103	200	78	3280	173	15	452	
hsa-miR-134-5p	207	548	407	415	880	799	535	2103	515	896	6
hsa-miR-136-3p	62	214	122	172	233	332	232	2203	87	267	1
hsa-miR-136-5p	29	74	51	49	28	83	205	141	84	71	1
hsa-miR-139-3p	880	1238	1035	875	2068	875	630	613	1042	1526	12
hsa-miR-139-5p	14828	27611	20023	18501	13303	20764	14400	7881	18597	42541	283
hsa-miR-140-3p	22945	44794	31782	35856	23411	69634	45181	86555	21726	48873	502
hsa-miR-140-5p	431	1228	1391	716	2071	1064	711	1138	699	1191	4
hsa-miR-142-3p	113	226	527	154	830	220	380	445	80	225	1
hsa-miR-142-5p	692	924	2293	840	4036	1572	1991	7380	579	1881	7
hsa-miR-143-3p	2015953	4556724	3320922	3879204	2860440	3712446	2242639	2292880	1567386	3897960	19725
hsa-miR-143-5p	1500	4432	4826	3138	3469	4477	2146	20137	1303	4522	15
hsa-miR-144-3p	32	34	246	82	376	91	251	2582	18	62	
hsa-miR-144-5p	201	406	857	222	1166	403	841	450	102	479	3
hsa-miR-145-3p	1031	2348	2806	1851	3751	2438	2462	5703	1860	3651	10
hsa-miR-145-5p	10972	55471	19317	26634	29947	32254	8631	115830	8427	17234	220
hsa-miR-146a-5p	6080	13366	5986	6569	6956	9781	13024	11949	5760	8172	152
hsa-miR-146b-3p	163	410	204	365	420	409	521	186	631	463	6
hsa-miR-146b-5p	8048	24407	12467	24078	49163	31768	20031	37545	34016	22672	218
hsa-miR-147b-3p	50	79	90	148	53	74	85	67	143	111	
hsa-miR-148a-3p	3563590	6850914	4666939	11088551	1650724	9286099	6480496	1776088	6719574	7188026	127378
hsa-miR-148a-5p	221	697	708	807	1035	763	538	3397	413	598	5
hsa-miR-148b-3p	28358	59037	35511	37134	39969	27703	34481	35545	42983	41434	307
hsa-miR-148b-5p	73	203	191	108	279	179	170	411	101	222	1
hsa-miR-149-5p	135	388	178	273	280	214	165	464	214	174	3
hsa-miR-150-3p	21	38	33	52	60	77	41	35	53	44	
hsa-miR-150-5p	1391	3434	3117	2332	6288	3258	1938	7559	2488	2384	24
hsa-miR-151a-3p	199946	273106	202812	502951	70444	390390	360395	196199	609689	364806	12896
hsa-miR-151a-5p	159	386	274	450	262	254	198	1021	355	221	4
hsa-miR-152-3p	23382	68286	44741	54594	65285	63755	51269	78859	46609	55198	600
hsa-miR-152-5p	14	111	36	54	101	71	21	1000	47	30	

hsa-miR-155-5p	792	1767	962	1253	1422	1475	1223	291	947	1679	16
hsa-miR-15a-5p	60	76	151	80	118	161	140	323	43	77	
hsa-miR-15b-3p	669	846	1522	1680	861	1724	1861	1096	326	895	9
hsa-miR-15b-5p	375	541	791	431	774	489	779	362	330	674	5
hsa-miR-16-2-3p	182	233	614	233	1082	389	421	466	159	378	3
hsa-miR-16-5p	1909	3807	5801	3801	6595	5534	4607	8692	1357	4633	28
hsa-miR-17-5p	376	823	1025	467	1570	846	919	2608	300	864	5
hsa-miR-181a-2-3p	264	596	806	589	741	596	303	388	430	544	7
hsa-miR-181a-3p	73	308	311	215	338	196	155	470	173	259	1
hsa-miR-181a-5p	1777	5494	6296	4619	12471	5400	3294	34731	3368	5719	34
hsa-miR-181b-5p	226	623	795	563	1359	769	370	2014	448	879	5
hsa-miR-181c-3p	34	63	63	76	107	108	47	680	64	114	
hsa-miR-181d-5p	137	319	235	281	353	424	130	690	141	377	2
hsa-miR-182-5p	12347	20934	22787	16538	17188	27612	32675	2398	9112	36800	331
hsa-miR-183-5p	1869	3405	4017	3024	3889	4720	4972	922	1682	6660	46
hsa-miR-184	81	109	8	56	23	104	116	97	36	53	1
hsa-miR-1843	106	209	143	168	164	114	122	132	214	244	2
hsa-miR-185-3p	229	482	380	445	472	291	353	700	222	438	2
hsa-miR-185-5p	2540	3257	6358	3407	14933	4167	6114	7363	1307	6873	18
hsa-miR-186-5p	1364	3505	3961	2560	5301	4383	3159	36392	1349	4048	17
hsa-miR-190a-5p	63	206	175	137	89	97	193	499	113	66	
hsa-miR-191-5p	4107	11362	10845	6166	19890	8071	10580	27139	10224	7812	88
hsa-miR-192-5p	1211	2365	2953	2028	5207	3107	2778	10020	1257	3260	19
hsa-miR-193a-3p	4	26	44	48	28	59	38	327	14	42	
hsa-miR-193a-5p	566	1201	1645	1276	2633	1328	868	1550	1326	1365	15
hsa-miR-193b-3p	415	1615	1257	924	1452	1603	572	6963	336	935	5
hsa-miR-193b-5p	124	216	304	275	407	305	212	105	179	260	2
hsa-miR-194-5p	146	297	448	281	642	293	415	1159	168	426	2
hsa-miR-195-3p	753	1854	1299	1443	2417	1210	842	1951	1653	2005	25
hsa-miR-195-5p	765	1575	1806	1335	2897	1929	1617	3483	961	2041	10
hsa-miR-196a-5p	382	1070	944	543	1629	1376	986	212	423	961	7
hsa-miR-196b-5p	303	919	619	619	1238	908	493	268	270	736	3
hsa-miR-197-3p	307	1011	646	583	1200	786	338	2081	543	668	5
hsa-miR-199a-5p	4620	22732	17538	15982	20384	27577	9759	171727	6528	18097	86
hsa-miR-199b-5p	23686	136656	47739	70638	47217	132558	48239	71509	32110	86407	560
hsa-miR-19a-3p	83	91	166	71	193	102	207	139	19	165	
hsa-miR-19b-3p	353	1015	531	580	844	719	748	1534	309	502	2
hsa-miR-200a-3p	42	230	108	364	568	111	328	612	79	368	2
hsa-miR-200a-5p	66	132	66	187	103	81	207	68	83	211	2
hsa-miR-200b-3p	99	289	203	161	883	143	244	171	67	363	15
hsa-miR-200c-3p	73	101	62	86	337	37	120	125	34	163	10
hsa-miR-203a-3p	142	100	43	237	245	43	30	195	35	446	2
hsa-miR-204-5p	166	711	1007	458	542	164	204	2640	321	312	3
hsa-miR-206	108	120	22	174	427	209	15559	23	31	3741	1
hsa-miR-20a-5p	479	881	1314	527	2584	875	899	5018	396	967	3
hsa-miR-20b-5p	39	129	145	72	289	85	141	270	21	84	
hsa-miR-21-3p	142	137	275	297	134	151	399	1389	286	179	
hsa-miR-21-5p	132985	369504	262072	224478	491979	348402	200712	307204	302170	353812	1778
hsa-miR-210-3p	181	567	276	249	513	310	266	911	302	235	2
hsa-miR-2110	68	107	79	83	244	99	99	42	43	129	
hsa-miR-212-5p	29	62	63	44	154	39	55	237	49	76	
hsa-miR-214-3p	211	768	586	650	546	1194	496	2096	391	631	6
hsa-miR-214-5p	210	703	686	613	456	1024	523	843	377	626	5
hsa-miR-215-5p	3841	5860	10787	12490	9967	11305	4801	10274	5339	12486	80
hsa-miR-218-5p	4624	11576	12524	16443	2294	11899	24261	7675	18212	10130	152
hsa-miR-22-3p	653	1194	2071	1394	4308	1593	1005	4714	847	1761	11
hsa-miR-22-5p	689	1376	1786	1388	2380	1624	1033	3840	1220	1581	7
hsa-miR-221-3p	1844	5508	3528	3285	5289	7280	2298	5194	1787	7797	36

hsa-miR-221-5p	736	2756	699	1107	743	1893	848	312	908	1490	14
hsa-miR-222-3p	1303	3716	2258	2287	3853	3894	1131	3502	1175	4579	21
hsa-miR-223-3p	743	1037	1970	780	2932	2459	1732	1051	1033	2997	14
hsa-miR-223-5p	104	126	417	128	590	358	362	54	245	406	2
hsa-miR-224-3p	39	139	121	88	132	142	80	187	75	126	
hsa-miR-224-5p	12079	37535	21861	27532	40562	15146	16426	74155	29103	31056	264
hsa-miR-23a-3p	14445	41099	34495	19551	44478	39768	26954	18804	20975	46709	279
hsa-miR-23a-5p	34	34	57	35	68	16	27	25	33	31	
hsa-miR-23b-3p	4507	15405	14626	6593	14871	13574	9494	8210	10210	16218	113
hsa-miR-23b-5p	12	35	47	27	68	41	52	37	44	66	
hsa-miR-24-1-5p	32	77	87	88	76	100	74	131	95	150	
hsa-miR-24-2-5p	351	767	661	517	947	606	551	2696	552	735	5
hsa-miR-24-3p	9956	26101	24054	20335	32153	21566	16720	34374	15244	26185	183
hsa-miR-25-3p	20816	35743	37086	29588	47427	21413	23986	43178	20640	36616	174
hsa-miR-26a-2-3p	46	130	91	78	105	85	109	21	63	98	
hsa-miR-26a-5p	131639	391706	322054	235287	612721	259804	316381	866375	261994	304085	2851
hsa-miR-26b-5p	16627	41188	39336	37825	41305	29664	47035	11342	34952	31722	420
hsa-miR-27a-3p	10172	18458	31583	25266	50112	31427	19229	335087	16799	31979	151
hsa-miR-27a-5p	4875	6536	6733	10174	13505	7255	3353	4115	3903	6121	42
hsa-miR-27b-3p	34405	88214	116358	72605	113959	94671	60711	247297	53142	99430	543
hsa-miR-27b-5p	132	321	432	236	463	244	213	224	316	429	2
hsa-miR-28-3p	11538	28560	14194	21863	16846	24804	17714	14409	18791	18920	407
hsa-miR-28-5p	138	377	376	239	746	373	272	646	285	391	2
hsa-miR-29a-3p	2279	7973	6165	5180	7634	10850	5190	57224	2547	6801	40
hsa-miR-29b-3p	376	972	1335	791	901	1323	995	3605	546	979	9
hsa-miR-29c-3p	103	317	353	353	202	778	312	4168	85	273	1
hsa-miR-29c-5p	805	2749	1562	2024	816	1846	1843	1934	2323	1133	29
hsa-miR-30a-3p	11415	25200	22393	24800	16111	31008	13104	6738	13035	23731	223
hsa-miR-30a-5p	70239	223948	193513	138483	95003	274340	172196	521357	125414	133917	1143
hsa-miR-30b-3p	35	51	40	37	191	55	50	77	44	102	
hsa-miR-30b-5p	1248	4699	4787	2682	3704	6149	2660	10846	1391	3802	21
hsa-miR-30c-1-3p	26	102	135	101	163	128	97	239	49	153	
hsa-miR-30c-2-3p	1728	4272	2978	3520	2461	3822	2307	2814	2487	2277	27
hsa-miR-30c-5p	3202	12209	10710	5663	19467	8722	5150	19249	6699	8344	68
hsa-miR-30d-3p	78	166	166	165	155	203	74	422	98	157	
hsa-miR-30d-5p	46157	130441	92515	56096	162361	111514	60197	153637	66089	102811	834
hsa-miR-30e-3p	8244	19116	12568	19996	15088	21396	15518	5495	11193	19145	218
hsa-miR-30e-5p	986	2949	3134	1840	4982	2170	2959	25656	1250	2128	7
hsa-miR-3158-3p	650	617	1034	680	359	1125	2160	123	527	1197	18
hsa-miR-3182	112	72	321	185	122	249	190	9224	96	57	
hsa-miR-3195	19	29	199	83	18	70	7	128	19	60	
hsa-miR-32-3p	16	35	32	24	56	69	36	3	33	52	
hsa-miR-32-5p	73	128	435	182	355	170	334	1426	46	222	
hsa-miR-320a-3p	2327	4487	4878	4001	9553	6049	3766	3010	2149	10116	55
hsa-miR-323a-3p	39	65	29	67	112	51	26	99	36	72	
hsa-miR-324-3p	37	92	65	53	42	129	39	269	7	90	
hsa-miR-324-5p	25	69	82	41	47	110	35	290	24	56	
hsa-miR-326	42	151	99	188	97	138	28	788	78	105	
hsa-miR-328-3p	378	993	885	589	1783	635	242	2553	444	648	5
hsa-miR-330-3p	38	96	56	66	148	58	24	91	46	67	
hsa-miR-330-5p	62	94	125	158	84	101	118	220	127	188	2
hsa-miR-331-3p	191	426	344	336	361	381	163	1534	142	329	2
hsa-miR-331-5p	65	151	131	134	105	129	104	98	81	167	
hsa-miR-335-3p	9857	20494	19872	14243	32234	12168	19726	6775	42163	24986	298
hsa-miR-335-5p	1021	1441	3391	1630	4126	2126	2999	2282	1338	3166	8
hsa-miR-337-3p	15	70	23	60	52	18	20	12	32	58	
hsa-miR-338-5p	13	40	54	28	116	37	28	30	23	54	
hsa-miR-339-3p	155	320	400	246	470	380	179	717	225	363	2

hsa-miR-339-5p	75	162	135	112	242	252	78	972	96	122	1
hsa-miR-340-3p	169	649	461	535	632	373	410	185	438	457	8
hsa-miR-340-5p	637	1740	2876	1152	3760	1789	1782	5515	725	2244	8
hsa-miR-342-3p	1013	3298	1324	2753	1520	2178	1605	6740	1503	2251	27
hsa-miR-342-5p	23	50	37	52	82	83	58	7	18	54	
hsa-miR-345-5p	119	284	315	316	298	370	172	1992	199	330	2
hsa-miR-34a-5p	253	909	454	646	457	886	561	849	431	451	6
hsa-miR-34c-5p	73	240	129	195	142	194	226	767	100	115	
hsa-miR-361-3p	1876	5312	4075	5359	5731	4756	2352	8823	4361	5465	53
hsa-miR-361-5p	222	573	596	345	949	610	427	1184	425	602	4
hsa-miR-3613-5p	247	385	460	391	420	774	388	19	226	1157	1
hsa-miR-3614-5p	13	29	25	29	42	24	21	144	33	36	
hsa-miR-3615	555	776	1736	762	1524	731	694	1030	1018	929	8
hsa-miR-362-5p	10	51	46	30	48	30	38	60	19	20	
hsa-miR-363-3p	1090	2382	3009	2764	4409	2420	3632	4974	1014	2256	29
hsa-miR-365a-5p	274	932	428	308	315	611	793	26	621	510	11
hsa-miR-365b-5p	88	197	168	127	111	126	196	22	335	127	4
hsa-miR-369-3p	7	41	13	43	53	27	32	9	29	61	
hsa-miR-369-5p	12	24	18	17	45	21	13	17	23	34	
hsa-miR-3690	64	114	17	35	31	26	36	32	54	56	
hsa-miR-370-3p	211	495	341	655	1031	575	488	966	584	1233	6
hsa-miR-372-3p	777	21	13	110	50	53	14	162	48	22	9
hsa-miR-374a-3p	1633	3796	3284	3173	2470	3023	3673	1206	2513	2984	15
hsa-miR-374a-5p	423	1457	1615	1283	1965	943	1346	3276	809	1301	5
hsa-miR-374b-3p	45	125	158	90	205	120	85	64	78	144	
hsa-miR-374b-5p	767	3080	2068	1451	4673	1851	1712	4184	1593	2445	16
hsa-miR-375-3p	15	140	57	278	497	50	254	88	35	223	17
hsa-miR-378a-3p	94251	190460	238608	272438	219498	240743	137373	550060	167553	223387	1833
hsa-miR-378a-5p	39	97	176	116	204	101	49	677	44	79	
hsa-miR-378d	53	175	178	261	237	199	132	1856	128	187	
hsa-miR-378i	34	63	64	79	56	119	60	116	86	87	
hsa-miR-379-5p	2047	6814	2897	6408	4827	6453	6469	2957	5665	6826	103
hsa-miR-381-3p	1596	6450	5208	8644	5375	6843	8287	23808	4535	7429	61
hsa-miR-382-3p	41	137	69	145	187	171	148	331	195	165	2
hsa-miR-382-5p	42	99	83	140	174	60	180	25	227	222	2
hsa-miR-3909	63	194	128	94	228	82	63	59	109	134	1
hsa-miR-3913-5p	75	181	130	234	84	257	251	71	148	193	2
hsa-miR-3928-3p	27	21	23	38	33	49	25	47	19	28	
hsa-miR-3934-5p	15	25	17	20	35	31	11	21	18	29	
hsa-miR-409-3p	273	656	445	534	826	455	469	243	927	886	11
hsa-miR-409-5p	19	131	57	59	94	81	78	209	73	98	
hsa-miR-411-5p	179	709	391	454	1116	669	640	3546	455	726	5
hsa-miR-421	88	213	164	157	220	160	153	1025	122	204	1
hsa-miR-423-3p	1279	3505	2396	2248	6383	2783	1160	7093	1465	3314	20
hsa-miR-423-5p	5469	9591	8764	9238	14437	8535	9630	4563	6984	11530	103
hsa-miR-424-3p	31	86	51	64	154	57	38	78	99	64	
hsa-miR-424-5p	13	53	54	68	123	37	37	243	43	53	
hsa-miR-425-3p	76	193	158	139	166	259	127	374	127	169	1
hsa-miR-425-5p	866	2429	1307	3164	645	3557	2442	616	2380	2046	51
hsa-miR-4286	55	106	121	152	84	265	63	431	58	149	1
hsa-miR-432-5p	21	39	23	30	71	82	77	37	31	112	
hsa-miR-4326	10	3	44	58	49	1	42	53	37	63	
hsa-miR-4421	19	54	119	40	46	35	15	46	39	50	
hsa-miR-4504	47	57	58	59	30	102	90	30	43	57	
hsa-miR-450a-5p	98	250	302	249	617	186	109	1113	171	335	1
hsa-miR-450b-5p	663	1122	1022	1269	1435	939	649	605	1258	1186	6
hsa-miR-451a	175189	187147	388731	235913	142053	486837	483518	107369	103630	362139	2996
hsa-miR-452-3p	149	439	454	358	477	398	266	1353	278	513	2

hsa-miR-452-5p	4746	11407	10691	8313	16366	8188	6802	17114	6469	11726	55
hsa-miR-4521	33	110	72	23	105	56	21	114	29	64	
hsa-miR-454-3p	129	309	305	131	354	314	281	49	174	264	1
hsa-miR-455-3p	93	443	266	421	223	406	101	513	242	259	2
hsa-miR-455-5p	628	1943	1297	1855	832	2667	1093	4230	1223	1391	10
hsa-miR-4661-5p	32	64	35	55	17	39	25	28	43	49	
hsa-miR-4662a-5p	15	20	23	30	66	18	36	26	39	24	
hsa-miR-4677-3p	120	194	113	155	124	146	132	74	135	111	1
hsa-miR-4709-3p	22	64	30	58	33	48	43	14	47	28	
hsa-miR-4791	241	24	255	579	99	397	337	803	112	352	
hsa-miR-483-5p	62	23	38	78	68	64	37	86	29	63	
hsa-miR-484	165	406	507	276	783	279	161	1800	188	326	2
hsa-miR-485-5p	34	97	44	69	133	122	109	51	83	238	1
hsa-miR-486-3p	44	74	140	58	318	18	109	78	37	181	
hsa-miR-486-5p	32542	42209	64718	37127	89902	64547	65567	48860	14632	66649	745
hsa-miR-487b-3p	11	40	23	20	48	34	32	22	55	63	
hsa-miR-491-5p	15	45	21	28	25	55	16	73	22	32	
hsa-miR-493-3p	25	77	52	109	101	101	159	59	102	249	2
hsa-miR-493-5p	58	159	105	107	452	121	261	4	216	369	2
hsa-miR-494-3p	23	105	61	48	189	74	65	110	60	84	
hsa-miR-495-3p	9	66	43	59	150	52	42	48	54	162	
hsa-miR-497-5p	58	223	241	132	387	225	139	2349	110	186	1
hsa-miR-499a-5p	18	41	86	60	82	66	351	213	47	105	
hsa-miR-500a-3p	465	1056	651	513	1257	637	419	1029	430	717	3
hsa-miR-501-3p	374	760	491	461	827	493	330	614	371	683	3
hsa-miR-5010-3p	119	408	187	289	193	286	135	100	145	171	3
hsa-miR-502-3p	131	289	372	174	420	322	270	290	175	608	2
hsa-miR-503-5p	96	135	155	159	224	99	164	268	50	136	
hsa-miR-504-5p	379	1360	1505	1014	1595	1270	574	1391	1105	984	9
hsa-miR-505-3p	57	203	106	90	264	74	60	206	165	117	
hsa-miR-511-5p	437	682	623	303	626	580	602	100	989	767	16
hsa-miR-514a-3p	30	70	53	40	14	73	95	63	29	35	
hsa-miR-516a-5p	10	53	31	31	235	57	27	301	45	26	
hsa-miR-516b-5p	252	748	416	575	1857	796	374	616	1047	518	6
hsa-miR-518b	28	68	26	54	179	94	8	169	55	42	
hsa-miR-532-3p	41	63	42	50	80	58	30	215	79	37	
hsa-miR-532-5p	9239	19782	11394	18650	12876	17177	13117	41197	13568	15830	201
hsa-miR-542-3p	306	457	542	722	587	623	508	1091	454	669	2
hsa-miR-548az-5p	13	86	25	56	61	35	50	0	14	62	
hsa-miR-548bc	34	48	70	37	85	59	54	84	31	64	
hsa-miR-548e-3p	34	53	80	33	116	73	83	126	31	87	
hsa-miR-548f-3p	39	90	64	82	88	80	59	100	33	83	
hsa-miR-548o-3p	415	1079	648	805	343	1006	1091	894	979	1047	14
hsa-miR-551b-3p	17	22	27	39	25	7	11	307	21	12	
hsa-miR-5683	21	135	488	46	114	199	1088	1489	63	143	
hsa-miR-574-3p	1836	4117	3496	3999	3135	6640	4639	4557	4661	3035	82
hsa-miR-574-5p	527	1326	926	931	1005	1324	1335	286	1271	1537	13
hsa-miR-576-3p	33	55	68	36	89	68	69	14	31	106	
hsa-miR-576-5p	28	80	47	44	100	45	62	20	63	64	
hsa-miR-582-3p	2672	2335	1806	3778	1010	3685	3270	681	1742	2639	22
hsa-miR-582-5p	29	74	33	42	39	90	92	76	32	72	
hsa-miR-584-5p	180	340	395	559	541	360	355	165	292	403	5
hsa-miR-585-3p	121	144	98	68	399	2842	1425	483	268	292	
hsa-miR-589-5p	404	813	608	1014	825	1471	382	3726	449	554	7
hsa-miR-590-3p	26	59	74	51	43	73	58	33	26	75	
hsa-miR-598-3p	21	32	48	43	83	43	28	119	45	89	
hsa-miR-615-3p	134	190	219	127	577	132	71	850	139	188	1
hsa-miR-625-3p	14	24	16	26	47	24	16	46	14	35	

hsa-miR-628-5p	26	50	41	33	70	49	50	56	49	60	
hsa-miR-629-5p	825	1683	1633	1464	2984	1982	1255	1953	667	2026	9
hsa-miR-6500-3p	28	105	409	94	111	99	47	675	119	148	
hsa-miR-651-5p	157	363	324	393	256	452	278	92	310	336	2
hsa-miR-652-3p	577	1380	2234	1272	1968	2248	1080	3474	804	1826	8
hsa-miR-652-5p	24	60	66	83	36	77	16	57	17	38	
hsa-miR-653-5p	97	177	117	103	266	105	136	378	94	112	
hsa-miR-654-3p	262	779	491	968	520	502	1388	527	1865	747	18
hsa-miR-654-5p	129	333	139	307	255	327	258	101	327	497	4
hsa-miR-659-5p	84	152	87	135	33	106	111	48	194	102	2
hsa-miR-660-5p	165	492	429	225	581	427	342	3804	174	345	1
hsa-miR-664a-3p	226	744	535	296	808	548	286	523	374	405	3
hsa-miR-664a-5p	119	205	287	173	597	474	355	64	122	463	3
hsa-miR-664b-3p	46	79	41	41	66	53	14	112	79	37	
hsa-miR-671-3p	58	91	100	111	138	99	41	204	131	67	1
hsa-miR-671-5p	9	38	29	17	45	37	11	50	24	19	
hsa-miR-6716-3p	50	73	97	68	144	48	45	281	100	43	
hsa-miR-675-3p	24	47	36	44	36	72	18	266	67	72	
hsa-miR-675-5p	5	58	17	25	36	17	17	47	52	28	
hsa-miR-6761-5p	5	41	47	42	49	62	34	19	43	46	
hsa-miR-6842-3p	92	152	141	198	65	212	109	41	173	178	5
hsa-miR-6866-5p	31	98	67	84	60	74	44	34	69	66	
hsa-miR-7-1-3p	23	50	45	35	27	41	31	80	15	35	
hsa-miR-7-5p	3670	9584	9957	5454	15450	9486	8920	1101	5222	13569	77
hsa-miR-708-3p	2961	4625	4125	11221	1519	9635	4123	6511	4930	6612	69
hsa-miR-708-5p	144	395	552	301	616	675	301	3487	267	459	1
hsa-miR-744-5p	1336	2336	2171	2245	3917	2616	1922	5676	2058	2554	24
hsa-miR-758-3p	14	78	39	69	100	97	51	225	95	83	
hsa-miR-760	19	14	54	25	77	52	13	40	19	48	
hsa-miR-769-5p	2874	6458	3334	5679	3535	6023	2786	11986	4592	3696	39
hsa-miR-7704	74	44	266	268	92	215	93	171	127	132	2
hsa-miR-7706	52	85	184	102	161	49	65	19	86	98	
hsa-miR-874-3p	69	175	96	100	244	169	67	781	97	117	
hsa-miR-889-3p	55	159	94	170	164	131	121	201	179	154	1
hsa-miR-891a-5p	32	98	64	99	56	67	81	38	42	46	2
hsa-miR-9-5p	42	186	123	120	396	59	54	56	78	172	2
hsa-miR-92a-3p	20312	42036	34881	24073	68454	20287	22040	24838	15834	26748	243
hsa-miR-92b-3p	179	671	278	147	644	233	178	434	314	328	2
hsa-miR-93-5p	1012	2661	2371	1272	3543	1807	1926	4089	982	2342	12
hsa-miR-941	1871	4367	2904	2346	3667	2424	2485	1438	4054	4633	45
hsa-miR-95-3p	1226	2492	2040	2021	3916	2109	2784	4472	1669	3534	22
hsa-miR-96-5p	85	179	269	105	153	174	156	37	44	266	
hsa-miR-98-3p	47	147	87	67	76	135	69	142	77	120	
hsa-miR-98-5p	1940	4735	5436	3250	8245	4522	5156	1133	3607	7623	30
hsa-miR-99a-3p	13	104	57	56	66	93	40	1059	27	43	
hsa-miR-99a-5p	90767	295763	280237	245465	231744	289137	296524	297796	246648	262395	3927
hsa-miR-99b-3p	2158	3916	3047	3848	2837	2752	2293	4805	4412	3739	47
hsa-miR-99b-5p	23090	52208	46544	38680	71618	31619	22277	75324	48777	35971	587

References

Andrews, S. et al. (2010). *FastQC: A quality control tool for high throughput sequence data*. Cambridge, United Kingdom.

Angulo, P. (2007). Obesity and nonalcoholic fatty liver disease. *Nutrition Reviews*, *65*(suppl_1), S57–S63.

Arrighetti, N., & Beretta, G. L. (2021). miRNAs as therapeutic tools and biomarkers for prostate cancer. *Pharmaceutics*, *13*(3), 380.

Caballería, L., Pera, G., Auladell, M. A., Torán, P., Muñoz, L., Miranda, D., Alumá, A., Casas, J. D., Sánchez, C., Gil, D., et al. (2010). Prevalence and factors associated with the presence of nonalcoholic fatty liver disease in an adult population in spain. *European Journal of Gastroenterology & Hepatology*, *22*(1), 24–32.

Carlson, M. (2024). *Org.hs.eg.db: Genome wide annotation for human*.

Carpentier, A. C. (2021). 100th anniversary of the discovery of insulin perspective: Insulin and adipose tissue fatty acid metabolism. *American Journal of Physiology-Endocrinology and Metabolism*, *320*(4), E653–E670.

Chan, W.-K., Chuah, K.-H., Rajaram, R. B., Lim, L.-L., Ratnasingam, J., & Vethakkan, S. R. (2023). Metabolic dysfunction-associated steatotic liver disease (MASLD): A state-of-the-art review. *Journal of Obesity & Metabolic Syndrome*, *32*(3), 197.

Chen, S., Zhou, Y., Chen, Y., & Gu, J. (2018). Fastp: An ultra-fast all-in-one FASTQ preprocessor. *Bioinformatics*, *34*(17), i884–i890.

Chen, Y., Chen, L., Lun, A. T. L., Baldoni, P., & Smyth, G. K. (2024). edgeR 4.0: Powerful differential analysis of sequencing data with expanded functionality and improved support for small counts and larger datasets. *bioRxiv*. https://doi.org/10.1101/2024.01.21.576131

Cinti, S. (2007). The adipose organ. *Adipose Tissue and Adipokines in Health and Disease*, 3–19.

Cinti, S. (2019). Anatomy and physiology of the nutritional system. *Molecular Aspects of Medicine*, *68*, 101–107.

Danecek, P., Bonfield, J. K., Liddle, J., Marshall, J., Ohan, V., Pollard, M. O., Whitwham, A., Keane, T., McCarthy, S. A., Davies, R. M., & Li, H. (2021). Twelve years of SAMtools and BCFtools. *GigaScience*, *10*(2). https://doi.org/10.1093/gigascience/giab008

Desvignes, T., Loher, P., Eilbeck, K., Ma, J., Urgese, G., Fromm, B., Sydes, J., Aparicio-Puerta, E., Barrera, V., Espin, R., et al. (2020). Unification of miRNA and isomiR research: The mirGFF3 format and the mirtop API. *Bioinformatics*, *36*(3), 698–703.

Duncan, R. E., Ahmadian, M., Jaworski, K., Sarkadi-Nagy, E., & Sul, H. S. (2007). Regulation of lipolysis in adipocytes. *Annu. Rev. Nutr.*, *27*(1), 79–101.

Ewels, P., Magnusson, M., Lundin, S., & Käller, M. (2016). MultiQC: Summarize analysis results for multiple tools and samples in a single report. *Bioinformatics*, *32*(19), 3047. https://doi.org/10.1093/bioinformatics/btw354

Friedman, J. (2019). *Leptin and the endocrine control of energy balance. Nat. Metab. 1, 754–764.*

Gesta, S., & Kahn, C. R. (2017). White adipose tissue. *Adipose Tissue Biology*, 149–199.

Ghesmati, Z., Rashid, M., Fayezi, S., Gieseler, F., Alizadeh, E., & Darabi, M. (2024). An update on the secretory functions of brown, white, and beige adipose tissue: Towards therapeutic applications. *Reviews in Endocrine and Metabolic Disorders*, *25*(2), 279–308.

Grabner, G. F., Xie, H., Schweiger, M., & Zechner, R. (2021). Lipolysis: Cellular mechanisms for lipid mobilization from fat stores. *Nature Metabolism*, *3*(11), 1445–1465.

Ibrahim, M. M. (2010). Subcutaneous and visceral adipose tissue: Structural and functional differences. *Obesity Reviews*, *11*(1), 11–18.

Idilman, I. S., Ozdeniz, I., & Karcaaltincaba, M. (2016). Hepatic steatosis: Etiology, patterns, and quantification. *Seminars in Ultrasound, CT and MRI*, *37*, 501–510.

Ipsen, D. H., Lykkesfeldt, J., & Tveden-Nyborg, P. (2018). Molecular mechanisms of hepatic lipid accumulation in non-alcoholic fatty liver disease. *Cellular and Molecular Life Sciences*, *75*, 3313–3327.

Jialal, I., & Devaraj, S. (2018). Subcutaneous adipose tissue biology in metabolic syndrome. *Hormone Molecular Biology and Clinical Investigation*, *33*(1), 20170074.

Kang, W., Eldfjell, Y., Fromm, B., Estivill, X., Biryukova, I., & Friedländer, M. R. (2018). miRTrace reveals the organismal origins of microRNA sequencing data. *Genome Biology*, *19*, 1–15.

Karbowska, J., & Kochan, Z. (2006). Role of adiponectin in the regulation of carbohydrate and lipid metabolism. *Journal of Physiology and Pharmacology*, *57*, 103.

Kershaw, E. E., & Flier, J. S. (2004). Adipose tissue as an endocrine organ. *The Journal of Clinical Endocrinology & Metabolism*, *89*(6), 2548–2556.

Koenen, M., Hill, M. A., Cohen, P., & Sowers, J. R. (2021). Obesity, adipose tissue and vascular dysfunction. *Circulation Research*, *128*(7), 951–968.

Kwok, K. H., Lam, K. S., & Xu, A. (2016). Heterogeneity of white adipose tissue: Molecular basis and clinical implications. *Experimental & Molecular Medicine*, *48*(3), e215–e215.

Langmead, B., Trapnell, C., Pop, M., & Salzberg, S. L. (2009). Ultrafast and memory-efficient alignment of short DNA sequences to the human genome. *Genome Biology*, *10*, 1–10.

Lopez-Yus, M., Hörndler, C., Borlan, S., Bernal-Monterde, V., & Arbones-Mainar, J. M. (2024). Unraveling adipose tissue dysfunction: Molecular mechanisms, novel biomarkers, and therapeutic targets for liver fat deposition. *Cells*, *13*(5), 380.

Love, M. I., Huber, W., & Anders, S. (2014). Moderated estimation of fold change and dispersion for RNA-seq data with DESeq2. *Genome Biology*, *15*, 550. https://doi.org/10.1186/s13059-014-0550-8

Ma, Y., Wang, J., Xiao, W., & Fan, X. (2024). A review of MASLD-related hepatocellular carcinoma: Progress in pathogenesis, early detection, and therapeutic interventions. *Frontiers in Medicine*, *11*, 1410668.

Mary, E., Jeffrey, V., Ratziu, V., Sven, M., Arun, J., Kanwal, F., Romero, D., Manal, F., Quentin, M., Arab, J. P., et al. (2024). A multisociety delphi consensus statement on new fatty liver disease nomenclature. *Annals of Hepatology*, *29*(1), 1–15.

McQuaid, S. E., Humphreys, S. M., Hodson, L., Fielding, B. A., Karpe, F., & Frayn, K. N. (2010). Femoral adipose tissue may accumulate the fat that has been recycled as VLDL and nonesterified fatty acids. *Diabetes*, *59*(10), 2465–2473.

Miao, L., Targher, G., Byrne, C. D., Cao, Y.-Y., & Zheng, M.-H. (2024). Current status and future trends of the global burden of MASLD. *Trends in Endocrinology & Metabolism*.

Morgan, M. (2024). *BiocVersion: Set the appropriate version of bioconductor packages*. https://doi.org/10.18129/B9.bioc.BiocVersion

Paik, J. M., Henry, L., Younossi, Y., Ong, J., Alqahtani, S., & Younossi, Z. M. (2023). The burden of nonalcoholic fatty liver disease (NAFLD) is rapidly growing in every region of the world from

1990 to 2019. *Hepatology Communications*, *7*(10), e0251.

Pantano, L., & Escaramis, G. (2024). *isomiRs: Analyze isomiRs and miRNAs from small RNA-seq*. https://doi.org/10.18129/B9.bioc.isomiRs

Peltzer, A., Trigila, A., Pantano, L., Ewels, P., Wang, C., Espinosa-Carrasco, J., Schcolnicov, N., Mohr, C., bot, nf-core, Menden, K., Patel, H., Sturm, G., CKComputomics, Cabus, L., Keys, K. L., Guizard, S., Garcia, M. U., Syme, R., Talbot, A., … Tommaso, P. D. (2024). *Nf-core/smrnaseq: v2.4.0 - 2024-10-14 - gray zinc dalmation patch*. Zenodo. https://doi.org/10.5281/ZENODO.3456879

Posit team. (2023). *RStudio: Integrated development environment for r*. Posit Software, PBC. http://www.posit.co/

R Core Team. (2024). *R: A language and environment for statistical computing*. R Foundation for Statistical Computing. https://www.R-project.org/

Rosen, E. D., & Spiegelman, B. M. (2014). What we talk about when we talk about fat. *Cell*, *156*(1), 20–44.

Ru, Y., Kechris, K. J., Tabakoff, B., Hoffman, P., Radcliffe, R. A., Bowler, R., Mahaffey, S., Rossi, S., Calin, G. A., Bemis, L., & Theodorescu, D. (2014). The multiMiR r package and database: Integration of microRNA target interactions along with their disease and drug associations. *Nucleic Acids Research*, *42*(17), e133. https://doi.org/10.1093/nar/gku631

Ru, Y., Mulvahill, M., Mahaffey, S., & Kechris, K. (n.d.). *multiMiR: Integration of multiple microRNA-target databases with their disease and drug associations*. https://github.com/KechrisLab/multiMiR

Santulli, G. (2015). *MicroRNA: Basic science: From molecular biology to clinical practice* (Vol. 887). Springer.

Saponaro, C., Gaggini, M., Carli, F., & Gastaldelli, A. (2015). The subtle balance between lipolysis and lipogenesis: A critical point in metabolic homeostasis. *Nutrients*, *7*(11), 9453–9474.

Sarwar, R., Pierce, N., & Koppe, S. (2018). Obesity and nonalcoholic fatty liver disease: Current perspectives. *Diabetes, Metabolic Syndrome and Obesity: Targets and Therapy*, 533–542.

Scheja, L., & Heeren, J. (2019). The endocrine function of adipose tissues in health and cardiometabolic disease. *Nature Reviews Endocrinology*, *15*(9), 507–524.

Scherer, P. E. (2006). Adipose tissue: From lipid storage compartment to endocrine organ. *Diabetes*, *55*(6), 1537–1545.

Song, Z., Xiaoli, A. M., & Yang, F. (2018). Regulation and metabolic significance of de novo lipogenesis in adipose tissues. *Nutrients*, *10*(10), 1383.

Thyfault, J. P., & Rector, R. S. (2020). Exercise combats hepatic steatosis: Potential mechanisms and clinical implications. *Diabetes*, *69*(4), 517–524.

Wong, R. J. (2024). Epidemiology of metabolic dysfunction-associated steatotic liver disease (MASLD) and alcohol-related liver disease (ALD). *Metabolism and Target Organ Damage*, *4*(4), N–A.

Xu, S., Hu, E., Cai, Y., Xie, Z., Luo, X., Zhan, L., Tang, W., Wang, Q., Liu, B., Wang, R., Xie, W., Wu, T., Xie, L., & Yu, G. (2024). Using clusterProfiler to characterize multiomics data. *Nature Protocols*. https://doi.org/10.1038/s41596-024-01020-z

Younossi, Z. M. (2019). Non-alcoholic fatty liver disease–a global public health perspective. *Journal of Hepatology*, *70*(3), 531–544.

Younossi, Z. M., Golabi, P., Avila, L. de, Paik, J. M., Srishord, M., Fukui, N., Qiu, Y., Burns, L., Afendy, A., & Nader, F. (2019). The global epidemiology of NAFLD and NASH in patients with type 2 diabetes: A systematic review and meta-analysis. *Journal of Hepatology*, *71*(4), 793–801.

Younossi, Z. M., Golabi, P., Paik, J. M., Henry, A., Van Dongen, C., & Henry, L. (2023). The global epidemiology of nonalcoholic fatty liver disease (NAFLD) and nonalcoholic steatohepatitis

(NASH): A systematic review. *Hepatology*, *77*(4), 1335–1347.

Younossi, Z. M., Koenig, A. B., Abdelatif, D., Fazel, Y., Henry, L., & Wymer, M. (2016). Global epidemiology of nonalcoholic fatty liver disease—meta-analytic assessment of prevalence, incidence, and outcomes. *Hepatology*, *64*(1), 73–84.

Younossi, Z., Anstee, Q. M., Marietti, M., Hardy, T., Henry, L., Eslam, M., George, J., & Bugianesi, E. (2018). Global burden of NAFLD and NASH: Trends, predictions, risk factors and prevention. *Nature Reviews Gastroenterology & Hepatology*, *15*(1), 11–20.

Zwick, R. K., Guerrero-Juarez, C. F., Horsley, V., & Plikus, M. V. (2018). Anatomical, physiological, and functional diversity of adipose tissue. *Cell Metabolism*, *27*(1), 68–83.